



Brigitte Schober, BSc

**Development of a mobile electro-mechanical test bench  
to investigate muscle behavior  
in lower limbs**

**MASTER'S THESIS**

to achieve the university degree of

Diplom-Ingenieurin

Master's degree programme: Biomedical Engineering

submitted to

**Graz University of Technology**

Supervisor

DI Christoph Leitner

DI Dr.techn. Christian Baumgartner

Institute of Health Care Engineering,  
Graz University of Technology

Graz, November 2020

## EIDESSTÄTLICHE ERKLÄRUNG

### **AFFIDAVIT**

Ich erkläre an Eides statt, dass ich die vorliegende Arbeit selbstständig verfasst, andere als die angegebenen Quellen/Hilfsmittel nicht benutzt, und die den benutzten Quellen wörtlich und inhaltlich entnommenen Stellen als solche kenntlich gemacht habe. Das in TUGRAZonline hochgeladene Textdokument ist mit der vorliegenden Masterarbeit/Diplomarbeit/Dissertation identisch.

*I declare that I have authored this thesis independently, that I have not used other than the declared sources/resources, and that I have explicitly indicated all material which has been quoted either literally or by content from the sources used. The text document uploaded to TUGRAZonline is identical to the present master's thesis/diploma thesis/doctoral dissertation.*

24.11.2020

Datum / Date

Schuber-Bergthaler

Unterschrift / Signature

*Die Technische Universität Graz übernimmt mit der Betreuung und Bewertung einer Masterarbeit keine Haftung für die erarbeiteten Ergebnisse: Eine positive Bewertung und Anerkennung (Approbation) einer Arbeit bescheinigt nicht notwendigerweise die vollständige Richtigkeit der Ergebnisse.*

## Acknowledgments

At this point I would like to thank everyone who supported me during the implementation of this master's thesis.

I would like to express my sincere gratitude to my supervisors DI Christoph Leitner and Univ.-Prof. DI Dr.techn. Christian Baumgartner for the excellent support and the time they made available. Mr. Leitner had a lot of patience and provided me with valuable knowledge for my project. Through regular consultations I received useful tips, which gave me new perspectives on certain content.

Furthermore I would like to say thank you to my parents, my sister and my boyfriend who shared their support during my whole studies, morally, financially and physically.

# Zusammenfassung

## Entwicklung eines mobilen elektro-mechanischen Prüfstandes um das Muskelverhalten in den unteren Gliedmaßen zu untersuchen

Die Kontraktion von Muskeln kann einerseits mit Oberflächen-Elektromyographie und andererseits mit Ultraschall untersucht werden. Mit einem Elektromyogramm ist es möglich, die Aktivierung, also die Aktionspotentiale der motorischen Einheit an der Hautoberfläche zu messen. Mit Ultraschall kann die daraus resultierende Muskelbewegung aufgenommen werden. Im Zuge dieser Masterarbeit wurde ein System entwickelt, um ein Ultraschallbild und ein hochdichtes Oberflächenelektromyogramm zugleich aufzunehmen. Außerdem wurde eine mobile und billige Variante eines Prüfstandes entwickelt, mit dem es möglich war, den medialen Gastrocnemius Muskel während einer freiwilligen maximalen Kontraktion zu untersuchen. Es konnte gezeigt werden, dass es möglich ist, Ultraschallbilder und hochdichte Elektromyographie Signale zur gleichen Zeit aufzunehmen. Bei beiden Techniken konnte eine gute Auflösung erzielt werden.

**Schlüsselwörter:** Ultraschall, Hochdichte Oberflächen-Elektromyographie, ultraschalltransparent, Bewegungsapparat, Kopplung

## Abstract

### Development of a mobile electro-mechanical test bench to investigate muscle behaviour in lower limbs

The contraction of muscles can be investigated on the one hand, with surface electromyography, which is a possibility to measure the muscle activation, so the motor unit action potentials on the skin surface, and on the other hand with ultrasound, where the resulting muscle movement can be mapped. In this master's thesis a hardware development was done, to combine these two modalities, so to acquire US and high-density surface electromyography simultaneously. Furthermore a mobile and low-cost solution of a test bench was designed and built, to investigate the medial gastrocnemius muscle during an isometric maximum voluntary contraction. It can be shown that it is possible to record ultrasound and high-density surface electromyography data in synchronized mode, with reasonable resolutions.

**Keywords:** ultrasound, high density surface electromyography, ultrasound transparent, musculoskeletal, coupling

# Contents

<b>1</b>	<b>Introduction</b>	<b>6</b>
<b>2</b>	<b>Literature review</b>	<b>9</b>
2.1	Muscle Anatomy and Functionality . . . . .	9
2.1.1	Muscle Structure and Morphology . . . . .	9
2.1.2	Electrical behaviour . . . . .	11
2.1.3	Motor Unit . . . . .	12
2.2	Ultrasound . . . . .	14
2.2.1	Physical Principles of Ultrasound . . . . .	14
2.2.2	2D B-mode Ultrasound . . . . .	15
2.3	Electromyography . . . . .	16
2.4	Parallel Ultrasound and EMG acquisition . . . . .	19
<b>3</b>	<b>Objective</b>	<b>20</b>
<b>4</b>	<b>Material and Methods</b>	<b>21</b>
4.1	Experimental Setup . . . . .	21
4.2	Ultrasound Setup . . . . .	22
4.3	Hardware . . . . .	24
4.3.1	Analog Hardware . . . . .	24
4.3.2	Digital Hardware . . . . .	25
4.4	Software . . . . .	26
4.4.1	Ultrasound Processing . . . . .	26
4.4.2	HDsEMG Processing . . . . .	26
4.4.3	Test Bench Processing . . . . .	27
4.5	Statistics . . . . .	28
<b>5</b>	<b>Results and Discussion</b>	<b>29</b>
5.1	Developed Hardware . . . . .	29
5.1.1	Ultrasound Transparent EMG Electrode Array . . . . .	29
5.1.2	EMG Acquisition Device . . . . .	33
5.1.3	Mobile Test Bench . . . . .	34
5.2	Verification of Hardware and Signals . . . . .	38
5.2.1	Ultrasound-Transparent Material . . . . .	38
5.2.2	Biosignal Verification of the US Transparent EMG Electrode . . . . .	40
5.2.3	EMG Acquisition Device . . . . .	41
5.2.4	Mobile Test Bench . . . . .	43
5.3	Measurement of Human Muscle Contractions In Vivo . . . . .	43
5.3.1	Measurements on Biceps Brachii . . . . .	43
5.3.2	Measurement on Medial Gastrocnemius . . . . .	47
5.4	Discussion . . . . .	52
<b>6</b>	<b>Conclusion</b>	<b>54</b>

# 1 Introduction

Locomotion derives from the Latin words *locō* (place) and *mōtiō* (to move) and refers to directional movement that enables someone or something to move from one location to another [1]. Locomotion is based on a process called stretch–shortening cycle (SSC), which is the combination of eccentric (elongation) and concentric (shortening) actions in muscle tissues [2].

In 1887, British photographer and pioneer in motion studies, Eadweard Muybridge, published a paper called *Animal Motion* [3], which broke new ground in terms of locomotion. Leland Stanford developed a camera, that made it possible to make sequential recordings of fast movements. Muybridge did thousands of photographic movement studies of healthy and diseased humans and animals with this camera. One of his most famous studies is shown in figure 1 [1].

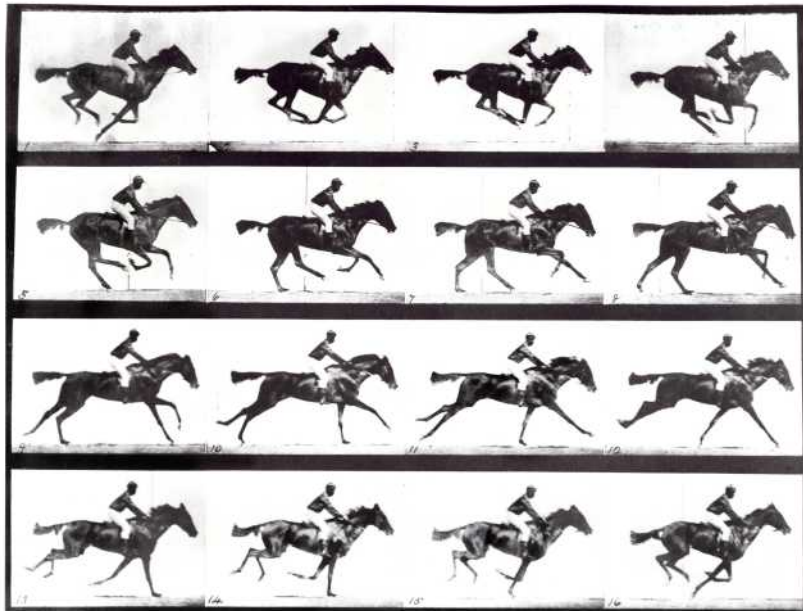


Figure 1: Eadweard Muybridge, photographic movement studies of a horseman and his horse [3]

Muscle force during human locomotion mainly depends on the grade of activation [4], the muscle length [5] and the rate at which the muscle changes its length [6]. Structural models, such as the Hill type muscle model (figure 2) are a commonly used way to abstract human muscle function. It consists of three types of elements, a contractile element (CE), a serial element (SE) and a parallel element (PE).

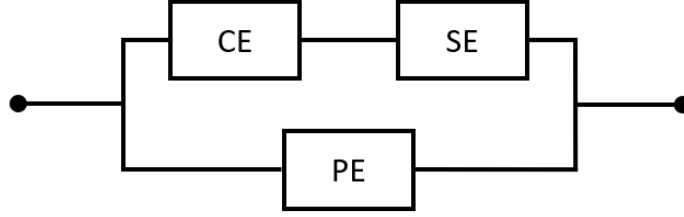


Figure 2: Muscle model by A. V. Hill, 1938 [6]

The SE and PE components represent the passive soft connective tissue including the tendons and inactive muscle fibers and the CE component describes the active muscle fibers. The active CE components are responsible for force generation. They are summarized by two properties, the force-length relationship and the force-velocity relationship. The force-length relationship says, the bigger the deviation of the muscle fibers from their rest length is, the less force can be applied. The force-velocity relationship says that in addition to the fiber length, muscle strength also depends on the velocity at which the muscle contracts. If the velocity is at its maximum, the force that is generated approaches to zero [6].

However, the experimental data-collection for these mathematical models is complex and limited mainly to the recording of peak isometric forces during maximum voluntary contractions in laboratory settings. Especially for the control of human machine interfaces (HMI), more general strategies are needed. HMI controls rely mainly on electromyographic data collected with small miniaturized devices. However, the derivation of muscles forces solely from electromyography (EMG) data is prone to errors [7]. Therefore, this thesis proposes an experimental method to collect both electromyographic (by EMG) and muscle length data (by ultrasound) in synchronized mode. The synchronized collection of muscle activation and length can assist the parameterization of future muscle models or HMI controls.

Ultrasound (US) is a low-risk, non-invasive, painless and radiation-exposure-free imaging technique for internal body structures such as tendons, muscles, blood vessels, and internal organs. In 1880, the Curie brothers laid an important foundation stone for technical echography with the discovery of the piezoelectric effect. During the First World War, this discovery showed its historical significance, as submarines could be located and destroyed using US. In 1928, S.Sokolov developed ultrasonic material testing methods using the transmission method. The next form of US application was in therapy. In 1939, R. von Pohlmann published a paper about the treatment of epicondylitis of violinists. The Austrian neurologist K. Th. Dussik was the first who used ultrasound for diagnostic purposes. In 1942, he published his method of hyperphonography for assessing the cerebral ventricles. From the beginning of the 1980s, the next generation of ultrasound devices brought a breakthrough and ultrasound was able to find its way into many specialist areas. In the 1990s, ultrasound as a research tool found its way into movement science [8].

Electromyography on the other hand, measures the electrical activity of muscles. Currents, generated in a muscle by a voluntary contraction, were registered for the first time in frogs by Carlo Matteucci in 1843 and in humans by DuBois-Reymond in 1851. Sherrington and Liddell introduced the concept of motor unit in 1925, which was essential for understanding the origin of the registered electrical signals. Since the fifties, Fritz Buchthal has established a standardization of the examination methods. The normal values, published by Buchthal [9], are still in use today [10].

The aim of the thesis is the simultaneous acquisition of ultrasound and high density surface EMG and so the combination of the modalities EMG and US to investigate a muscle contraction. EMG acquisition is supposed to be used to record the activation of the muscle. During US scan, the size and the resulted muscle movement during force generation can be seen. For better understanding, the context and purpose of this thesis, chapter 2, gives a literature overview on that topic. The objectives can be found in chapter 3. Chapter 4 describes the applied methods and gives an overview on hardware and software components used during this work. In chapter 5 the results are presented and discussed. Finally, a conclusion is given in chapter 6.

In the course of this thesis, the author also participated in the submission of a paper called "A Non-Invasive, Multimodal Method to Investigate Muscle Functions in Hind Limbs of Canine", in which a one channel US-EMG-electrode was applied on the medial gastrocnemius muscle in dogs, during treadmill walking. [11]

## 2 Literature review

### 2.1 Muscle Anatomy and Functionality

The human body has more than 650 muscles, which, together with bones, joints, tendons and ligaments form the supporting apparatus and the musculoskeletal system. Muscle tissue is one of the four basic tissue types of a human body. A distinction is made between skeletal muscle, cardiac muscle, and smooth muscle. They are all excitable, which means that the plasma membranes of the muscle can change their electrical state, from polarized to depolarized and send an action potential, which is an electrical wave, along the entire length of the membrane.

In the further course only skeletal muscles are considered, because the application of this research is done on this muscle group. The only possibility to contract a skeletal muscle is through a signal from the nervous system, unlike the others [12].

#### 2.1.1 Muscle Structure and Morphology

The skeletal muscle consists of various integrated tissues, including muscle fibers, nerve fibers, blood vessels, and connective tissue. In figure 3 and figure 4, the structure of a skeletal muscle is illustrated.

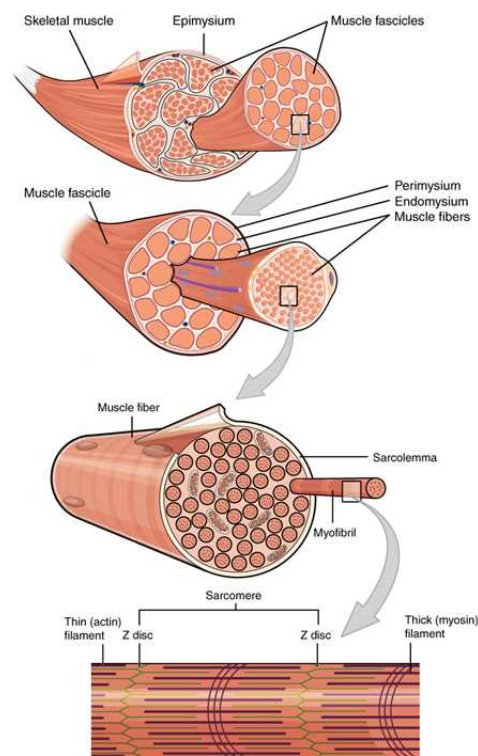


Figure 3: Structure of a skeletal muscle [12]

The **sarcomere**, the smallest functional unit of a skeletal muscle fiber for producing force, is a highly organized arrangement of contractile myofilaments **actin** and **myosin**, combined with other supporting proteins. The actin myofilaments are anchored at the so-called **Z-discs**. So the sarcomere is the region between two Z-discs. The sarcomeres are composed in series to the **myofibril**. The myofibrils run in parallel at the entire length of the muscle fiber [12]. E.g., in medial gastrocnemius muscles they are  $51 \pm 0.98$   $\mu\text{m}$  long with a diameter of 1-2  $\mu\text{m}$  [13]. The **sarcolemma** is the plasma membrane of muscle fibers. The action potential propagates along this membrane [12].

**Muscle fibers** are composed of myofibrils in parallel and have a diameter of 20-100  $\mu\text{m}$  [13]. A **fascicle** is a bundle of up to 150 parallel muscle fibers. These bundles are covered with a layer of **perimysium**, a connective tissue. Each individual muscle fiber is encased in **endomysium**. The **epimysium** wraps around each muscle and allows it to contract, while maintaining its structural integrity. It also separates the muscle from its surrounding organs and tissues to allow independent movements [12].

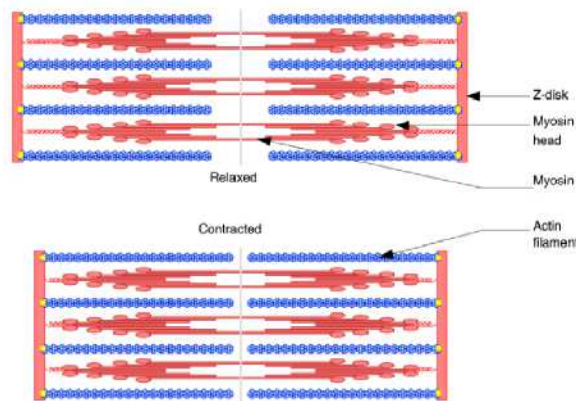


Figure 4: Schematic representation of a sarcomere during relaxation and contraction [5]

In the Huxley muscle model [5], the processes during force production at the sarcomere level of skeletal muscles are described. During contraction, actin and myosin slide into each other, without changing their own length (see figure 4). The myosin has small extensions ("heads") that can change their angle to the rest of the molecule ("shaft"). The heads can bind via cross bridges to the actin filaments and move them in "rowing movements". The contraction is triggered by a nerve impulse. To release myosin from actin, energy in the form of ATP is required. [5]

To maximize efficiency, muscles have different external shapes and internal architectures. An important factor is the organization of muscle fibers. Some muscles, like biceps brachii, have fibers, that run along the long axis of the muscle. A few fibers run over the entire length of the muscle, others are arranged in series and connected through

connective tissue. These so-called "parallel muscles", as seen in figure 5 on the left side, can have a long excursion, but only exert moderate force.

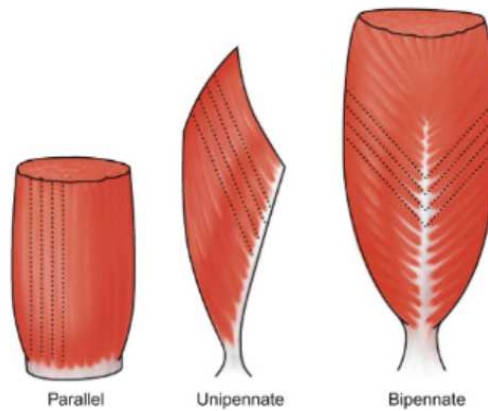


Figure 5: Types of internal architectures in muscles  
Modified from [14]

In contrast, pennate muscles have shorter fibers that are situated at an angle to the long axis of the muscle. The fibers are arranged in a feather-like structure. They can generate higher forces, but the excursion of these muscles is less. Unipennate muscles, like the medial gastrocnemius, have one row of oblique muscle fibres (see figure 5). Bipennate muscles consist of two rows of oblique muscle fibres, converging on a central tendon, facing in opposite diagonal directions. An example for a bipennate muscle is the rectus femoris. [14]

### 2.1.2 Electrical behaviour

The resting membrane potential of a muscle cell is about  $-70\text{mV}$  to  $-90\text{mV}$  inside the cell, with respect to the extracellular environment. This potential is kept up by sodium-potassium pump. This pump is working against the concentration gradient of ions flowing through the membrane and so mediates the maintenance of this potential. [15]

In the resting phase 3  $\text{Na}^+$  ions are pumped outside the cell during 2  $\text{K}^+$  ions are pumped inside the cell (figure 6 left side). After the muscle gets the message from the brain via the nerves to contract, calcium channels are opened on the terminal of the nerve fiber. The calcium binds to the vesicles filled with acetylcholine on the presynaptic membrane, which opens and releases the acetylcholine into the synaptic cleft. Acetylcholine migrates to the membrane of a muscle fiber, connects to the sodium-potassium pump and opens them. Depolarization takes place and  $\text{Na}^+$  flows into the cell and irritates it (figure 6 middle) . The membrane potential gets positive, up to  $+30\text{mV}$ . This

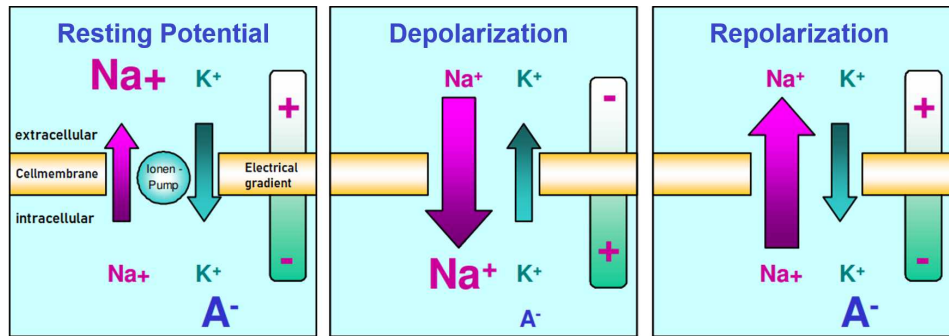


Figure 6: Flow of sodium and potassium during depolarization and repolarization of a muscle cell. Modified from [16]

leads to an activation of the ATPase. After splitting the ATP, the actin filaments slide between the myosin filaments and the muscle contracts as described in above. [12] [17] After that a repolarization takes place, where  $\text{Na}^+$  flows outside the cell (figure 6 right side). The membrane potential nearly approaches the resting potential, but it gets a little more negative, because the  $\text{K}^+$  channels are slightly delayed in closing. A short overshoot occurs, called hyperpolarization.

This temporary, characteristic deviation of the membrane potential from the resting potential is called action potential (AP). [12] The shape of an AP is illustrated in figure 7.

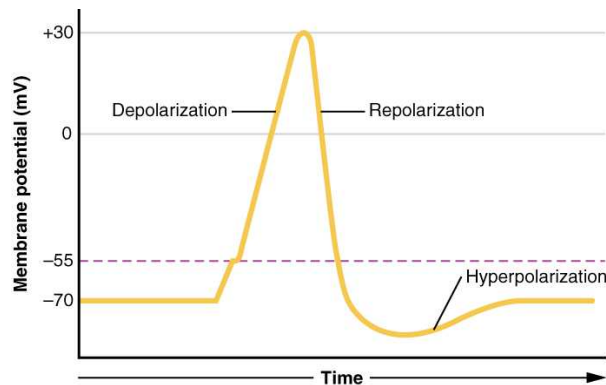


Figure 7: Action potential [12]

A sufficiently strong nerve stimulus contracts the muscle fiber maximally (all-or-nothing rule), then the muscle needs a recovery time for a few milliseconds during which it cannot be excited again. The strength of the overall contraction depends on how many motor units are excited. [18]

### 2.1.3 Motor Unit

A motor unit (MU) consists of a motor neuron and the skeletal muscle fibers, innervated by that neuron. The power performance of a muscle depends on the size and number of

the activated MU. Tailored to the function and the necessary force-intensity steps of a skeletal muscle, they differ in terms of the total number of their motor units and in the number of muscle fibers innervated per motor neuron. Smaller MUs consist of 100 to 300 muscle fibers, bigger MUs have up to 2000 fibers. [18] The MU is the smallest functional unit that can be controlled separately by the central nervous system. So the signal to innervate the muscle fiber is generated from the motor neuron, once it discharges. Consequently the AP starts at that connection and propagates toward the fiber end in both fiber directions similar but inverted, at a velocity of about 2-7m/s. The connection between motor neuron and muscle fiber is called neuromuscular junction or motor end plate (MEP). [19] In figure 8 this propagation is illustrated. [20]

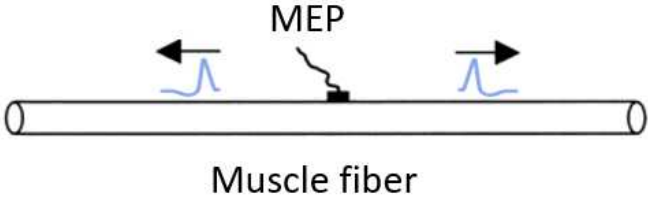


Figure 8: Propagating of an AP over a muscle fiber. Modified from [20]

An AP is formed almost simultaneously on every muscle fiber of the MU. The AP's, generated by the individual muscle fibers, build an algebraic summation in space and time, and generate the so-called motor unit action potential (MUAP), which can be derived electromyographically [19].

## 2.2 Ultrasound

Ultrasound is a versatile medical imaging tool. It is portable, non-invasive and operates without radiation exposition. It is a convenient method to visualise muscle movement and tissue structures. US has already been obtained with high spatial resolutions down to  $5 \mu\text{m}$  [21]. The resolution of a common US device, is in the sub-millimeter range depending on the used frequencies. Individual muscle fibers have a diameter between about  $40\mu\text{m}$  and  $80\mu\text{m}$ . This means, that either a fascicle or a small group of fibers is the smallest structure, that can be visualized with US. [22]

### 2.2.1 Physical Principles of Ultrasound

To generate an US image an acoustic pulse is emitted by an US transducer into the body part to be investigated. [23] The acoustic pulse is generated by piezoelectric materials, sitting inside of a transducer. In an US transducer an electrical high frequency impulse is transformed to a pressure wave by the use of this material. These pulses get partially reflected and scattered, due to interfaces of materials with different acoustic properties. The echo is again obtained by the piezoelectric material and transformed into an electrical signal. This method is called "Pulse-echo method". Subsequently the electrical signal gets amplified and can be displayed in different ways. [24] One of these ways is the 2D B-mode, explained later in this chapter.

An important property for the sound propagation in any material is the acoustic impedance. It can be explained by the resistance, that counteracts the sound waves. It depends on density and stiffness of a material. In the pulse echo method of medical ultrasound transducers the speed of sound is assumed to be constant at  $1450\text{ms}$ . This allows the depth detection of any arbitrary point in the ultrasound field through the collection of the reflecting pressure waves. A reflecting interface is necessary to produce an echo. Such an interface is generated in a human or animal body through the junction of tissues with different physical properties. The acoustic impedance  $Z$  of a material can be calculated as follows:

$$Z = \rho * c \quad (1)$$

$\rho$  is the density of the material and  $c$  is the propagation velocity of sound inside the material [24] [25].

If the difference of the acoustic impedances  $Z$  of the two materials, forming an interface, is high, waves cannot enter and are reflected. On the other hand if the impedance differences are small, waves are passing the interface [24] [25]. This relation is represented by the following formula for the reflection  $R$ :

$$R = \frac{(Z_2 - Z_1)^2}{(Z_2 + Z_1)^2} \quad (2)$$

$Z_1$  and  $Z_2$  are the acoustic impedances of two materials, that build an interface.

Table 1: Acoustic impedances of certain materials. Modified from [25]

Tissue	$Z$ in $\frac{kg}{m^2s}$
Air	$0.0004 * 10^6$
Water	$1.48 * 10^6$
Fat	$1.34 * 10^6$
Blood	$1.65 * 10^6$
Muscle	$1.71 * 10^6$
Bone	$7.8 * 10^6$

In table 1, it can be seen that  $Z$  of water, fat, blood and muscle is very similar, which means that the reflection at a surface of two of these medias is very small. In contrast, the difference of  $Z$  between for example air and muscle tissue is very high. With equation 2 an  $R$  of about 99% can be calculated :

$$R = \frac{(1.71 * 10^6 - 0.0004 * 10^6)^2}{(1.71 * 10^6 + 0.0004 * 10^6)^2} = 0.9991 = 99,91\% \quad (3)$$

This means that nearly all sound (99,91%) is reflected on such an interface, and no sound is left to spread further in tissues. This is why US coupling gels are used to transfer more ultrasound waves from the transducer into the body [24].

### 2.2.2 2D B-mode Ultrasound

In this thesis realtime 2D B-mode US with a linear array has been applied to observe and investigate muscles.

B-mode (brightness mode) is the most common display format in US imaging. The echo intensity (height of the amplitudes of the reflected signals) is shown as variation in brightness. So every grey shade of a pixel in a B-mode US image is a measure for the amplitude of an echo at this point where areas of high reflectivity appear lighter. A 2D-B-Mode US image with different intensities is illustrated in figure 9.

2D realtime images are generated by multiple US pulses, which are collected in series of successive scan lines (see figure 9). The produced lines are combined to the final image. The image is synchronized in realtime.

In linear arrays a high number of piezo-elements are arranged in a line. The piezo-elements are fired in a sequence which generates a series of parallel ultrasound beams. Each pulse forms a line of sight perpendicular to the array. The focus depths can be adjusted by altering the firing sequence [24].

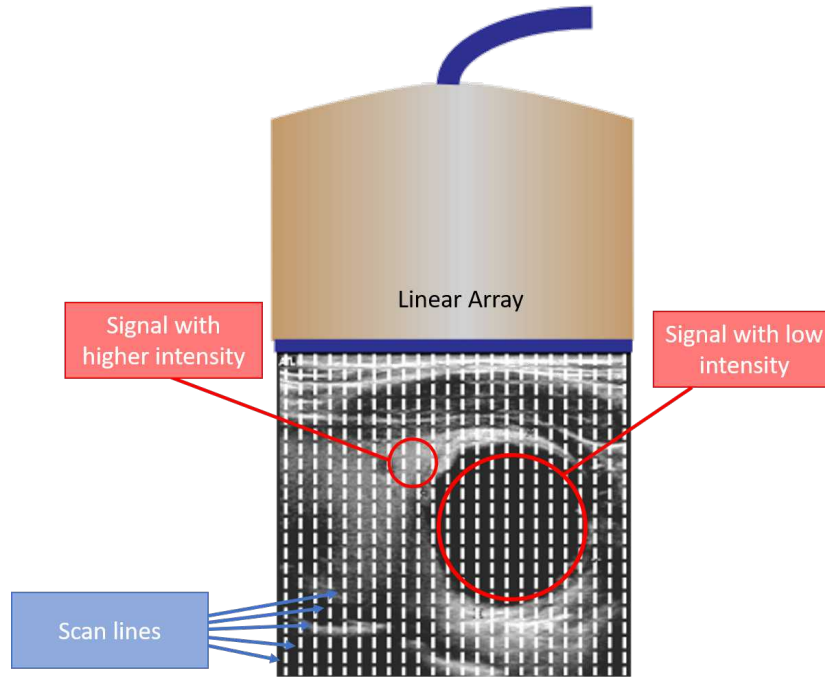


Figure 9: B-Mode US  
Modified from [24]

## 2.3 Electromyography

With an EMG it is possible to study the activation of a skeletal muscle through the recording of electrical potentials produced during muscle contractions (as described in chapter 2.1.2 and 2.1.3). It provides insights on the velocity and intensity of muscle contractions. Electrodes can be placed on the surface of the skin (surface electromyographie, sEMG) or inserted into the muscle tissue (intramuscular electromyography) [26]. Intramuscular EMG are widely used in clinical diagnostics. Due to its non-invasive nature, surface EMG is used for the works of this thesis.

The surface electromyography (sEMG) is a 2D distribution of the electric potentials, originated from the myoelectric activity of muscles, over the skin-surface. This analog signal is sampled in space, by the electrodes and in time, by the recording system [19]. Electric potentials have a frequency from about 15Hz to 400Hz. The amplitudes are in the range of micro- to millivolts peak to peak [26].

A potential difference between two electrodes is measured. One possibility is the monopolar detection (figure 10 (1)), where the signal between a sensing electrode, placed on the skin over the muscle, and a reference electrode is measured [26]. The reference electrode is usually placed on a skin area, that covers as few muscles as possible and is consequently an electrically uninvolved area, for example on the wrist or ankle [16]. An-

other detection technique is the single differential EMG, also called bipolar EMG (figure 10(3)). The potential difference between two monopolar EMGs ((1) and (2) in figure 10) is measured. The electrodes have to be placed in muscle fiber direction. While the monopolar derivation also records interferences from outside, as power line interference and activity of distant muscles, these interferences appear on bipolar technique with very similar amplitudes on both sensing electrodes and are consequently almost canceled out in the differentiated signal [26].

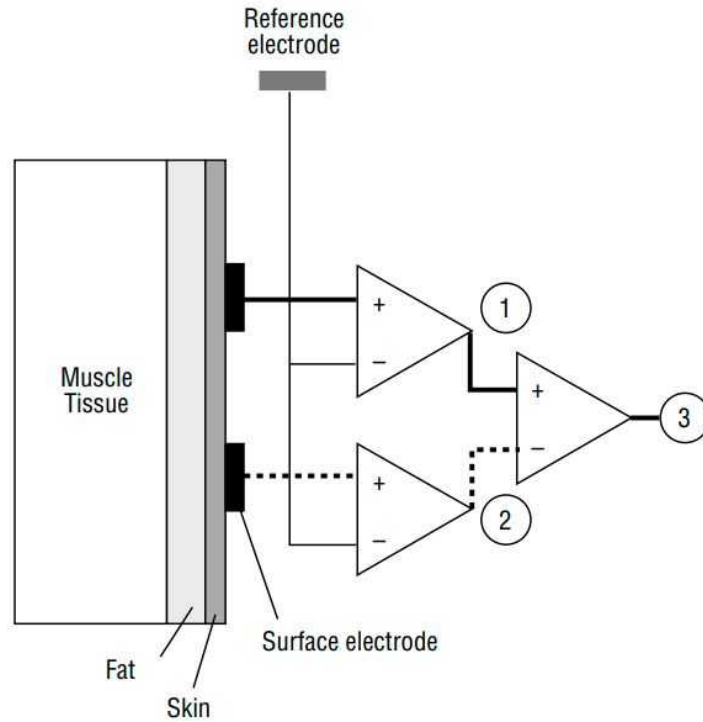


Figure 10: 1) and 2) Monopolar detection method 3) Bipolar detection method  
Modified from [26]

A third technique is the double differential detection, where a third electrode is added and the difference between two adjacent bipolar signals is computed. The contributions of interferences is consequently further reduced [27].

The generated AP is not only spread on muscle fibers, but is also transmitted through biological tissue. This phenom is called volume conduction and leads to a lowpass filtering on the transmitted signal [26]. The characteristics of this lowpass filter depend on electrode size and shape, inter-electrode distance, tissue composition and many other factors. As a consequence, the amplitude of the signal decreases and the signal bandwidth is reduced, with increasing thickness of the subcutaneous tissue layer and increasing inter-electrode distance [15].

For a HDsEMG, an array of multiple electrodes is used. This leads to a 3D sEMG image with two dimensions in space and one in time [28]. With this technique a clearly selected resolution can be reached, and individual MUAPs can also be measured non-invasively on the skin [15].

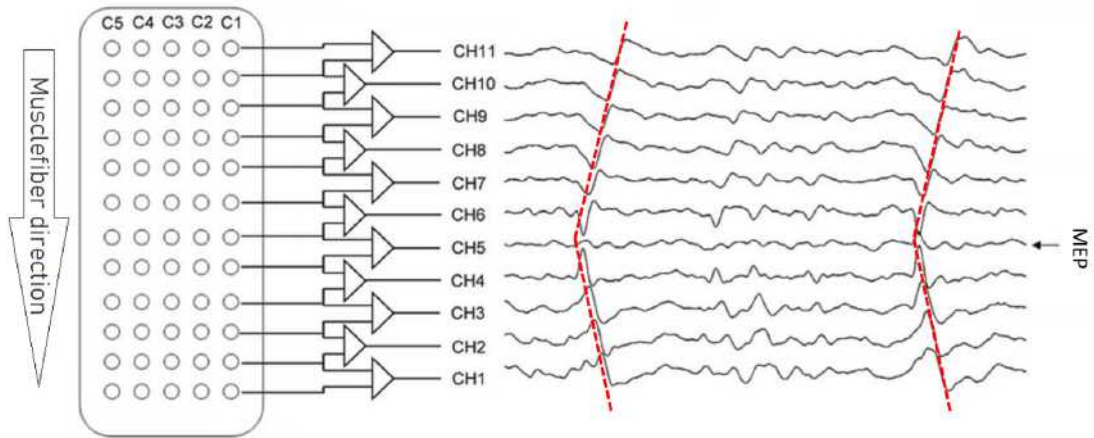


Figure 11: Electrode array for HDsEMG  
Modified from [29]

In figure 11 an electrode array is illustrated. All channels of one column are shown as triangle. On the right side examples for measured signals can be seen. The propagation of the AP can be recognized (marked by the red dashed lines). The MEP in this example is located at the level of CH5.

Merletti et al. [19] identified "compromise values" for inter-electrode distance (IED) and electrode diameter in HDsEMG. Compromise values mean that an alteration of results due to spatial filtering is moderate and acceptable. An electrode diameter  $d$  between 3mm and 5mm and an inter-electrode distance IED between 8mm and 10mm is recommended.

Based on this, the values in this thesis were chosen to:

$$d = 4mm$$

$$IED = 8mm$$

## 2.4 Parallel Ultrasound and EMG acquisition

Some researches on parallel US and EMG acquisition were already done in the past. Chen et al. [30] examined the relationship between muscle morphological changes derived from ultrasound image and the torque during isometric contraction of rectus femori and to compare it with relationship of torque and EMG and torque mechanomyography (MMG). Two standard surface EMG electrodes were placed at the two sides of the ultrasound transducer and in parallel with the muscle fibers. The MMG sensor was placed as near as possible to the distal EMG electrode.

Botter et al. [31] observed that for some body regions with small muscles and a high muscle density, the arrangement where the electrodes placed beside the US transducer is not viable, because the two investigation units would sample from different muscles. So they have previously shown the feasibility to captured the electromechanical behaviour of muscles using ultrasound and an electrode grid, transparent to ultrasound. They developed an US transparent EMG electrode. A layer of silicone rubber was used to embed a grid of electrodes. Each electrode consisted of a  $\text{Ø}0.1\text{mm}$  steel wire placed in a  $\text{Ø}0.4\text{mm}$  circular cavity in the layer. The grid consisted of 32 electrodes (4x8 array) with an IED of 10mm.

Furthermore Botter et al. [32] have developed a second solution for an EMG electrode transparent to US. Hydrogel was used as sensing region and for external structures. Since hydrogel is conductive, silicone rubber was used for the external electrode structure to isolate the two sensing regions from each other. The layer was designed with two electrodes for bipolar detection. The diameter of each electrode was 20mm and an IED was 3.5cm.

### 3 Objective

The aim of this master thesis is the development, design, engineering and verification of a mobile test bench to investigate muscle behaviour during an isometric maximum voluntary contraction, using a combination of high-density surface EMG (HDsEMG) and ultrasound (US). An ultrasound transparent HDsEMG system and a test bench should be developed and verified to record US, EMG and muscle force in a synchronised mode. Practical tests of human muscle contractions in vivo should be done.

Since the derivation of muscles forces solely from EMG data, like mainly used to control HMIs, is prone to errors, a method to collect both electromyographic (EMG) and muscle length data (ultrasound) in synchronized mode can assist future research in parameterization of muscle models or HMI controls.

## 4 Material and Methods

### 4.1 Experimental Setup

Due to the limitations in the laboratory because of the COVID 19 pandemic, only one proband was worked with. The proband was a 41 year old male with a high of 169cm and a weight of 69kg.

In the further course of this thesis two human muscles were investigated, the biceps brachii and the medial gastrocnemius. The biceps brachii is a skeletal muscle of the upper arm (see figure 12). It is a muscle with parallel muscle fibers and has two heads, the short head and the long head. Its functions include, for example flexion of the forearm and supination of the hand [17].

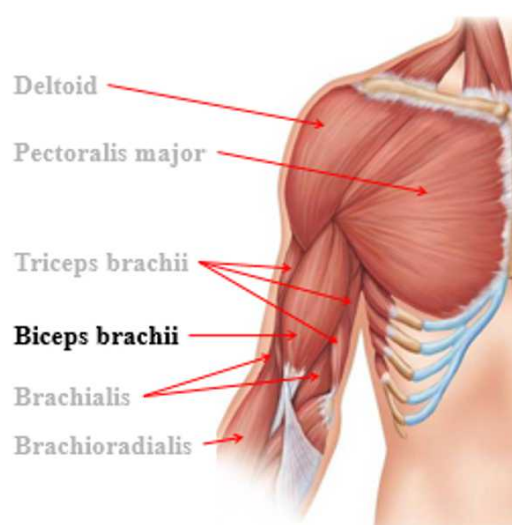


Figure 12: Anterior shoulder and arm with biceps brachii  
Modified from [17]

The gastrocnemius muscle is a superficial skeletal muscle in the lower leg. The muscle has two heads the Caput mediale (medial head) and the Caput laterale (lateral head). Its function includes for example the flexion of the knee joint and the plantarflexion [17].

The skin areas above the muscle, where the examination took place were prepared to get a better electrode skin contact and to reduce the skin-resistance. For this purpose, loose dander were removed by using fine sandpaper and alcohol.



Figure 13: Lower leg with gastrocnemius  
Modified from [17]

## 4.2 Ultrasound Setup

The General Purpose Ultrasound Phantom Model 054GS from CIRS was used for verification. The model is made of different wires, embedded in hydro gel polymer. The hydro gel polymer imitates human tissue while the wires give the possibility to verify lateral and axial resolution of US images. The phantom includes a fixture, where it is possible to fill in water between phantom and US probe. So there is no need to use ultrasound gel between probe and phantom. In figure 14 the inner structure of the phantom is visible. The area which is used to record US images later in this thesis (see chapter 5.2.1) is marked blue.

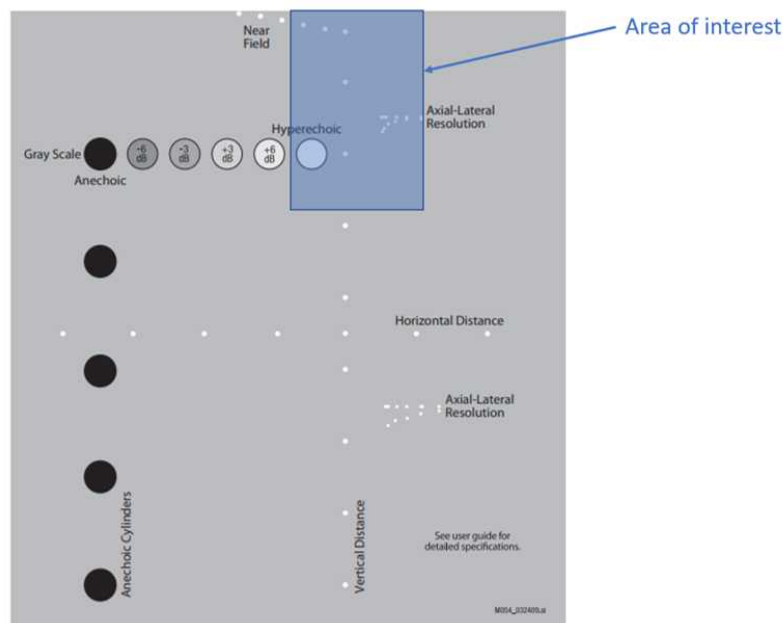


Figure 14: CIRS General Purpose Ultrasound Phantom Model 054GS

All ultrasound images in the course of this thesis were recorded with a portable ultrasound equipment, Mindray M5.



Figure 15: Ultrasound equipment Mindray M5

Mindray M5 is a portable diagnostic ultrasound system (see figure 15) which is suitable for musculoskeletal examinations. The US probe 7L4s from Mindray was used. The linear probe is able to emit frequencies between 5MHz and 10MHz. During investigations in the further course of the thesis a frequency of 5MHz was used. Four focus positions in the depths of 0.6cm, 1.2cm, 2cm and 2.8cm were set.

## 4.3 Hardware

### 4.3.1 Analog Hardware

The **INA114** is a general purpose instrumentation amplifier from Texas Instruments, offering a good accuracy. The schematic can be seen in figure 16. It is laser trimmed for a low offset voltage of maximal  $50 \mu\text{V}$  and a drift of maximal  $0.25 \mu\text{V}/^\circ\text{C}$ . It has a high common-mode rejection of minimal 115dB and a high input impedance of about  $10^{10}\Omega$ . It is possible to set a gain from 1 to 10000 with the external resistor  $R_G$ .

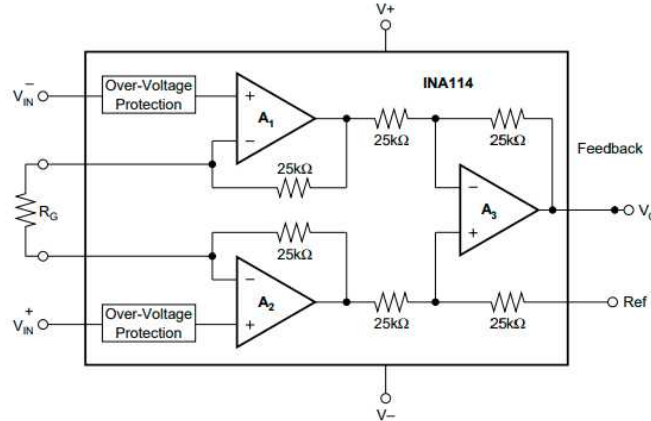


Figure 16: Schematic of INA 114AP

Furthermore the **TL081CP** from Texas Instruments was used as operational amplifier. It is a junction gate field effect transistor (JFET)-input operational amplifier. The device offers a low input bias current of 30 pA and a low input offset current of 5 pA. Because of the JFET input stage the operational amplifier has a high input impedance of about  $10^{12}\Omega$ . The common mode rejection ratio is about 86dB.

All used **resistors** are fixed carbon film resistors with axial connectors. A carbon film resistor is made of a ceramic substrate covered with a carbon film which has the desired resistance value. [33] The tolerance of this resistors is  $\pm 5\%$ . They offer a good long-term stability and generate little noise.

All **capacitors** are aluminum electrolytic capacitors with axial connectors. These types of capacitors are polarized. The anode is made out of aluminum foil. As dielectric acts a thin insulating layer of aluminum oxide on the aluminium foil. The cathode consists of an electrolyte. [33] The tolerance is  $\pm 20\%$ . This type of capacitors has a high electric strength and a compact design.

Two **S-load cells** from PSD (figure 17) were used in the test bench (see chapter 5.1.3) to measure muscle force. They had a rated load of 300kg each. Inside the S-load cells are strain gauges, which are combined in a bridge circuit. Strain gauges change their

electrical resistance at the slightest deformation, so the measuring of compression and tension is possible. The S-load cells have a high degree of accuracy and linearity.



Figure 17: Sload cell from PSD

Each setup was built up on a **breadboard**. A Conrad breadboard with 2700 poles was used for the EMG acquisition device. For the amplifier circuit of the test bench a mini breadboard from RND componets with 170 poles was used.

#### 4.3.2 Digital Hardware

**NI USB-6001** is a data acquisition (DAQ) devices from National Instruments. The full-speed USB device provides eight analog input channels, two analog output channels, 13 digital input/output channels, and a 32-bit counter. The analog-to-digital converter (ADC) resolution is 14 bit and the maximum sample rate is 20 kS/s. It can be controlled via LabVIEW (National Instruments, Austin, USA).

The **Arduino micro** (figure 18) is a microcontroller board based on the 8-bit microcontroller ATmega32U4. It has 20 digital input/output pins, 12 of them can also be used as analog inputs. It has a 16 MHz crystal oscillator and operates at 0V to 5V. It can be programmed via the Arduino Software IDE.

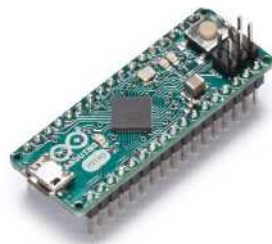


Figure 18: Arduino Micro

## 4.4 Software

### 4.4.1 Ultrasound Processing

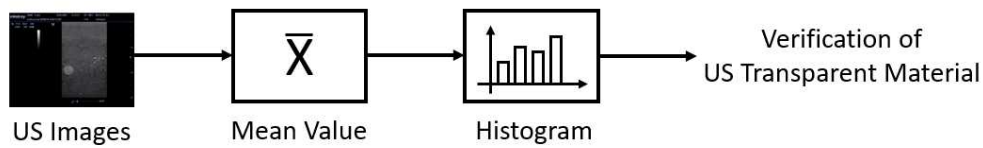


Figure 19: Signal processing for ultrasound images

US images under two different conditions were recorded from the blue marked area of the CIRS US phantom (see chapter 4.1). At first US images through a layer of US transparent material were recorded. Second, pictures were taken from the same area without the use of US transparent material. To compare these US images, at first a mean value of five US images per condition was built. The next step was to calculate histogram curves of 1D lines in five different depths. A histogram curve shows the distribution of the grey values. It is used to plot the number of pixel for each tonal value. The images of the two different sessions can be compared by observing the difference between these curves. Calculation and comparison were done in Matlab (Mathworks Inc., Natick, USA).

### 4.4.2 HDsEMG Processing

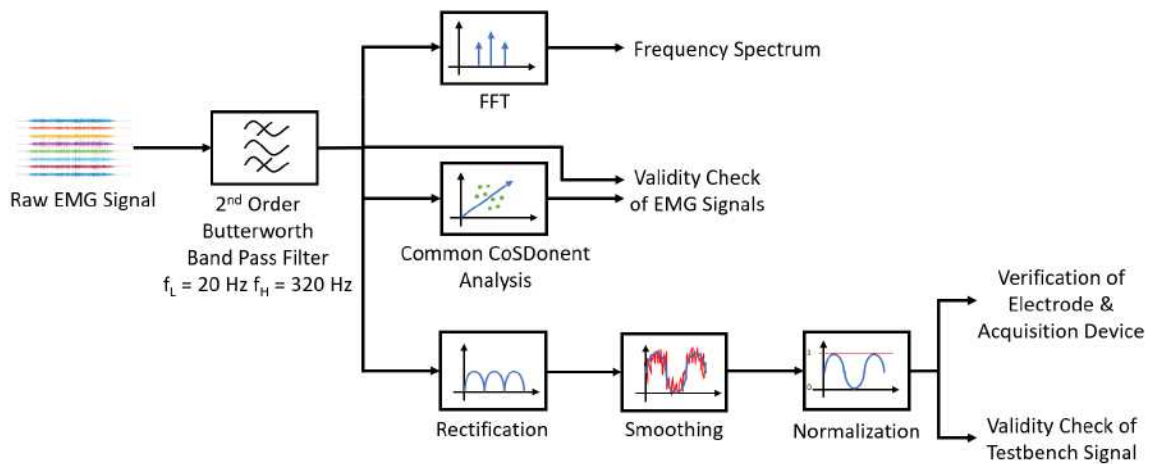


Figure 20: Three ways of signal processing for HDsEMG signals

LabVIEW (National Instruments, Austin, USA) was used to read-in the recorded EMG signals from the DAQ and save them in a text file. The further signal processing of these signals was done in Matlab (Mathworks Inc., Natick, USA). The processing included the following steps:

The first step was to filter the signals with a  $2^{nd}$  order butterworth band pass filter with a frequency range between 20 Hz and 320 Hz. The filter was provided in the course of the thesis. After filtering, three ways of signal processing were done:

- The first way was to perform a fast Fourier transformation (FFT) to get the frequency spectrum of the recorded signals (see figure 20, upper part of the diagram).
- The second way was to perform a CCA (Common CoSDonent Analysis) to check, if the recorded signal is valid (see figure 20, middle part). Common CoSDonent Analysis was programmed by H. Penasso and is based on a principal component analysis (PCA). Is the amplitude of the output curve of the analysis, named fcc, similar to the amplitude of the EMG signal, the change of the signal from one sampled point to the next sampled point is very large. This means that the noise component is very large and drowns out the EMG signal. If that is the case, the recorded signal is useless. The code to perform a CoSDonent Analysis was also provided in the course of the thesis.
- The last way was to rectify, smooth and normalize the band pass filtered signals (figure 20, lower part). This was done to get the basic course of each signal.

The calculation of the motor unit action potential (MUAP) propagation velocity was also done with a Matlab program, by using the method of D. Farina and R. Merletti. This Matlab program was provided in the course of this thesis.

#### **4.4.3 Test Bench Processing**

The output voltage of the S-loadcells was A/D converted by an Arduino micro. The associated program was written in Arduino IDE (Arduino SRL, Torino, Italy). If the EMG acquisition was started, a trigger-signal arrived from the NI 6001. Than the Arduino started to record the voltage values from the two S-load cells. The values were transmitted serially, until another trigger-signal was sent. The serial values were imported with a Matlab (Mathworks Inc., Natick, USA) program for further processing. The vectors of the two load cells were added and an offsest correction was done.

## 4.5 Statistics

1D statistical parameter mapping (SPM) was used to compare EMG signals, recorded from the same limb during two different conditions, one time to verify the EMG acquisition device and one time to verify the EMG electrode. In all cases it was hypothesized that the signals do not reveal significant differences. With a two sample T-Test, results were tested against the null hypothesis with a minimum level of statistical significance of  $p < 0.05$ . The two sample T-test was done in Matlab (Mathworks Inc., Natick, USA) with the SPM toolbox [34].

## 5 Results and Discussion

This chapter first describes and discusses the developed hardware. The hardware includes an EMG device which consists of two parts, the US transparent EMG electrode array and the EMG acquisition device. In addition a mobile and low-cost version of a test bench was developed and built, to get a repeatable setup for the investigation of muscle behavior of medial gastrocnemius during isometric plantarflexion. The second part of this chapter concentrates on presenting and discuss the signals which were recorded with this setup, for verification, validation, and for practical tests on a human proband.

### 5.1 Developed Hardware

#### 5.1.1 Ultrasound Transparent EMG Electrode Array

There was one requirement for the material of the EMG electrode array. The quality of the ultrasound image should be influenced as little as possible. To achieve this, the impedances of the muscle tissue and of the electrode array material have to match as good as possible (see chapter 2.2.1) and the air layers in and between the materials have to be reduced. A literature review (see chapter 2.4) has shown, that this can be achieved with silicones, especially duplicating silicones, used from dentists for the fabrication of negative forms. In the course of this thesis, three different silicones were investigated. Details about the used silicones can be found in Table 2.

Table 2: Different silicone- types, used in this thesis

Designation	Manufacturer	Color	Shore-Hardness
Technosil NT	Bredent Group	light-blue	25
Elite Double 8	Zhermack	pink	8
S-Trans Supersoft	TFC Troll Factory	transparent	0

An experiment was done to find out which silicon in which thickness is the most suitable. Different layers in different thicknesses and also combinations between two silicones were casted and US images were recorded through the layers. The result was, that the lower the shore hardness and the thinner the layer, the better the quality of the recorded US image.

For the first try to build an ultrasound transparent EMG-electrode, the Ag/AgCl-sensors of two adhesive electrodes were molded into a layer of Elite Double 8 (see figure 21, at the top). The advantage of this version was that the recorded EMG signal was good without much noise. The disadvantages were, on the one hand, that it was not possible to get a small IED, and so a HDsEMG was not possible. On the other hand, the US image was disturbed by the sensors, which can be seen in figure 21, top right.

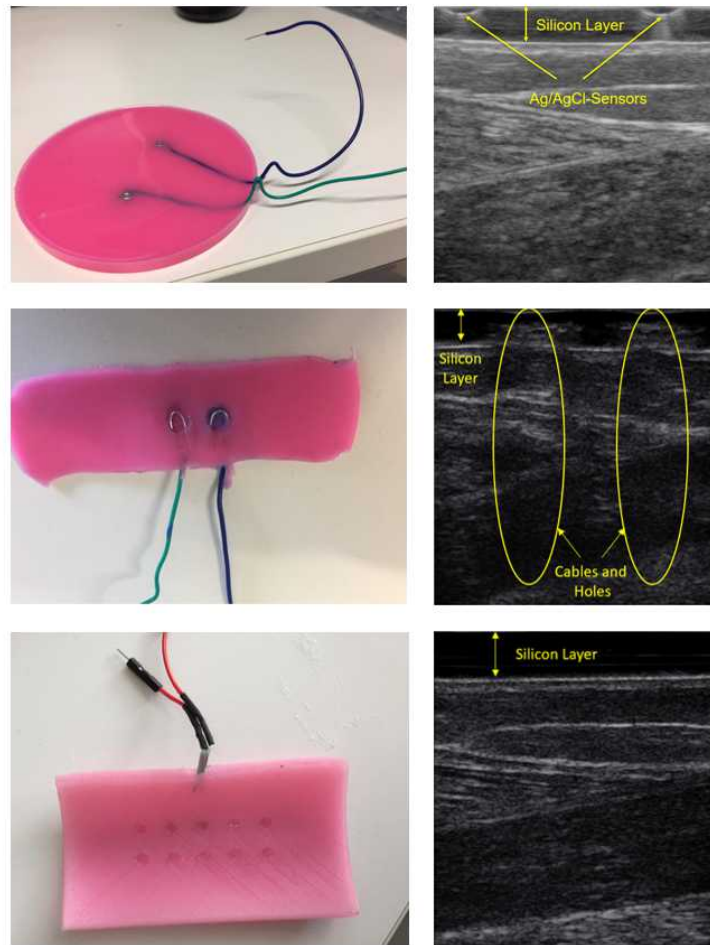


Figure 21: Left side: Previous solutions of US transparent EMG electrodes. Right side: Corresponding US image.

In the next stage, only stainless steel cables with a diameter of  $\text{Ø}2\text{mm}$  were used as sensors, and casted in an Elite Double 8 layer. Plasticine was used to build the form. One time the loose end of the cable was used, and one time a loop was formed to minimize the risk of injury by sticking with the end of the cable. Again the US image was disturbed by the cables. This version can be seen in figure 21 at the middle. A smaller IED was possible, but not small enough to get a HDsEMG. A huge amount of electrode gel was needed to get a good electrode skin contact and to fill the air gap to get a better US image. Nevertheless the cables and the air wholes are visible during US investigation (see figure 21, middle right).

So for the next stage a 3D printed mold was designed to cast an electrode array. As sensors, copper-wire braids were used. To get the layer as thin as possible, die casting was applied. The 3D-printed mold (see figure 22) was filled with the silicones via a syringe. The disadvantage of this method was, that there were many air bubbles inside

the material (figure 23). So for further processing, normal casting was done. The producing of such thin layers was not possible, but the advantage was, that there were no air bubbles inside the layers, causing the reflection of ultrasound.



Figure 22: 3D-printed die casting mold

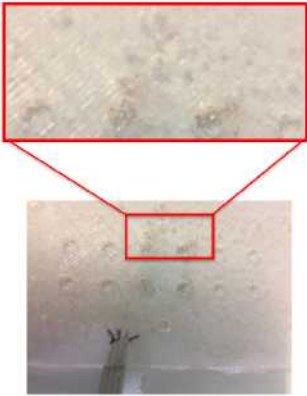


Figure 23: Air bubbles inside the cured silicone

The big advantage was that very small IEDs and electrode diameters were possible. Also, the wires did not disturb the US image. The only big disadvantage was that an exact positioning of the US-transducer on the array was not possible. Because of this, a redesign of the mold was done and the electrode was fixed directly on the transducer (see figure 25).

The mold of figure 24 was used to manufacture the final version of the ultrasound-transparent EMG electrode. At the bottom of the mold ten burlings were located, as counterforms of the electrodes.

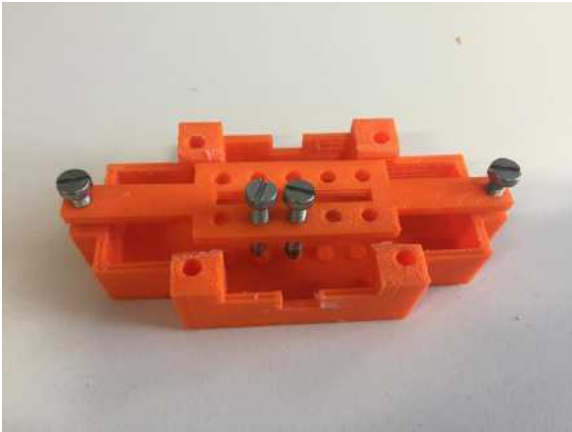


Figure 24: Final version of mold, used to cast the US-EMG electrode

The electrode was manufactured in seven steps:

1. Step one was to cast a layer as high as the burlings, of S-Trans supersoft silicon.
2. The next step was to embed ten copper- wire braids at the top of each burl. These braids are used as sensors. The wires had a diameter of  $\text{Ø}0,1\text{mm}$ .
3. After that the screws of the upper part were screwed down to fasten the braids on their positions.
4. Another layer of S-Trans supersoft was cast, on top.
5. The screws were unfastened and another thin layer of S-Trans supersoft silicon was cast to fill the resulting wholes.
6. While the previous layer was not completely cured, the 3D-printed adapter was placed inside the mold.
7. The last step was to pour the 3D printed adapter in with the Elite Double 8 silicone. The Elite Double 8 silicone was used as upper layer to get a more robust electrode, and to house the cables and the wire-cable connections. Furthermore the electrode was fastened on the adapter by this layer.

The result was a silicone layer with an array of 2x5 electrodes. Each electrode consisted of a copper wire braid, embedded in a circular cavity with a diameter of  $\text{Ø}4\text{mm}$ . The horizontal inter-electrode distance (IED) was 8mm, which is recommended for HDsEMG (see chapter 2.3). To locate the electrodes outside the field of view of the US transducer the vertical IED was chosen to be 11mm (see figure 26).

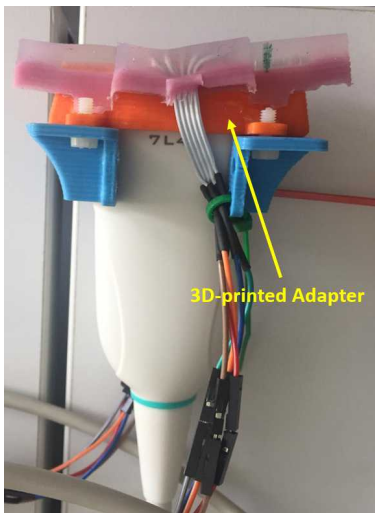


Figure 25: EMG electrode fixed on US transducer via 3D-printed adapter

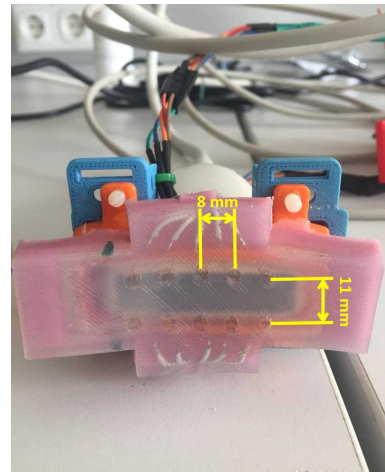


Figure 26: Inter electrode distances of the EMG electrode

### 5.1.2 EMG Acquisition Device

To record the EMG signals, an eight channel amplifier was designed. Each channel was designed as follows:

1. The first stage was an instrumentation amplifier INA 114 AP from Texas Instruments, used as pre-amplifier. The INA 114 AP was chosen, because it offers high accuracy and a high common-mode rejection. Also very important is the high input impedance. It ensures that signals are only minimally affected by a high skin-electrode resistance. The gain was set to  $G=51$  by an external resistor ( $R=1k\Omega$ ).
2. The second stage was a passive 1<sup>st</sup> order RC highpass filter with a cutoff-frequency  $f_c = 5\text{Hz}$ . To realize this, a  $100\text{ k}\Omega$  resistor was combined with a  $0,33\ \mu\text{F}$  capacity. The filter was used to remove the parasitic DC voltage and so to prevent the second amplification stage of saturation.
3. In this next amplification stage, a non-inverting amplifier, as operational amplifier a TL081CP from Texas Instruments was chosen. To get a gain of approximately 21, resistors  $R_1=20k\Omega$  and  $R_2= 1k\Omega$  were chosen.
4. The fourth stage was an active 2<sup>nd</sup> order Sallen Key lowpass filter with  $f_c=500\text{Hz}$ . It was designed with  $2x\ R=1\text{ k}\Omega$  and  $2x\ C=0,33\ \mu\text{F}$  . As operational amplifier also a TL081CP from Texas Instruments was used. The purpose of this filter was to avoid the aliasing effect.
5. The last stage of the EMG acquisition device was an analog to digital converter (ADC) to digitize the measured voltage. A National Instruments USB-6001 data acquisition (DAQ) device with a 14 bit resolution was used. LabVIEW (National Instruments, Austin, USA) was applied to read in and save the data in a text file. The sample-frequency  $f_s$  was set to  $1000\text{Hz}$ , to avoid aliasing. This program was also used to send a trigger signal to the arduino, in order to start and stop the recording of the test bench signal, and to synchronize both systems by doing so.

The total gain of the circuit was approximately 1071. All parts of the circuit were tested with the help of a signal generator and an oscilloscope. The schematic of one channel of the EMG acquisition device is shown in figure 27.

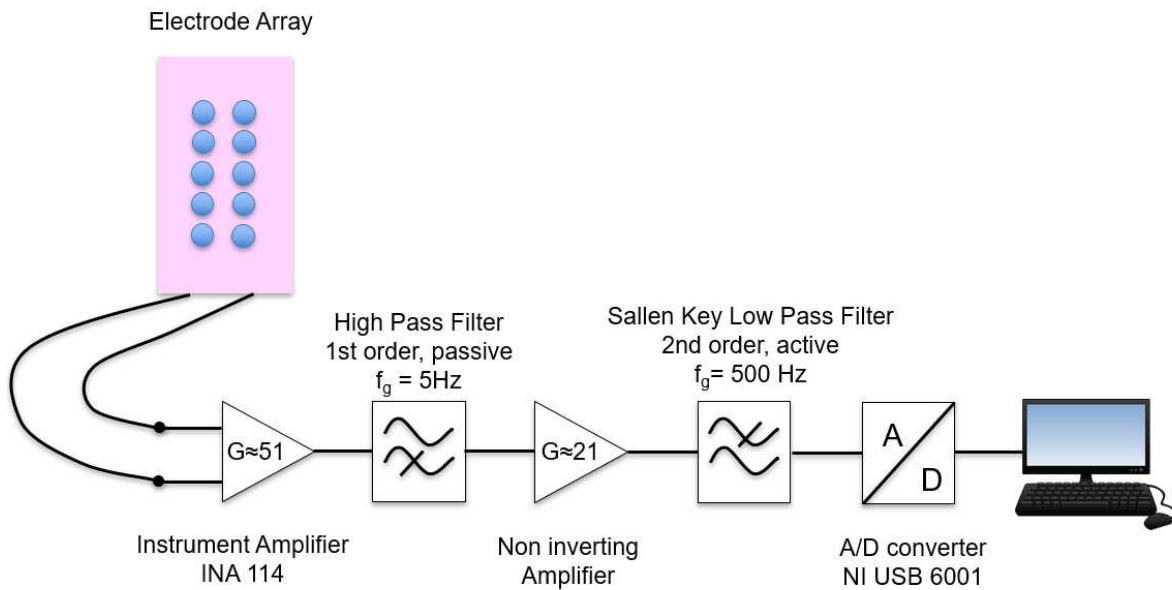


Figure 27: Schematic of one channel of the developed EMG acquisition device

### 5.1.3 Mobile Test Bench

In table 3 the way to the actual solution can be seen. In the first row the versions-number is visible. Row two describes, what has been changed since the last version. Row three shows the advantages of this version compared to the previous.

Table 3: Older Versions of the mobile test bench

Version	Update	Advantage
1	fix installed on a folding chair	mobile
2	mounted with two clamps	more mobile
3	added shoe	better fixed foot
4	thinner ground board	easier reach region to be investigated
5	seat belt instead of tension belt	better stability
6	S-load cells fixed between two ends of belt	force measurement is possible
End Version	S-load cells fixed on upper board	more stable

The final version of the mobile, low-cost test bench (figure 28) consisted of two wooden boards (1 is the upper-board, 2 is the ground-board), one hinge (3) with a removable bolt, one sandal (4), a velcro fastener (5) mounted in two eyelets (6), and a seat belt (7). Furthermore a squeeze buckle (8) connected the two ends of the seat belts, which allowed to adjust the length. The seatbelt was attached on both sides to a S-load cell (9) via a M12 screw (10) and the S-load cells were fixed on the wooden board with one M12 screws each as well. The test bench can be mounted with two clamps (11) on any chairs or similar.

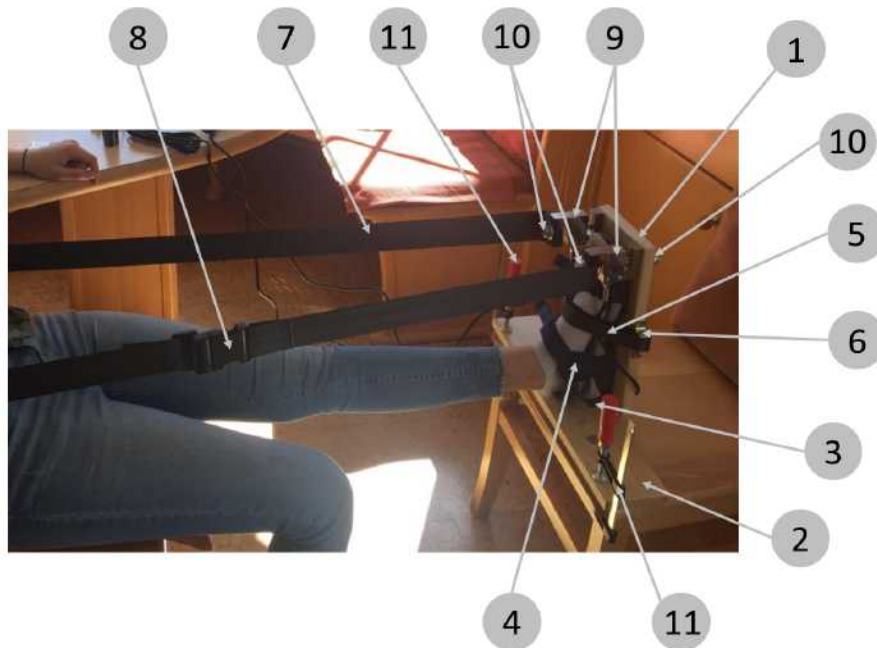


Figure 28: Final version of the mobile test bench

The hinge with the removable bolt and the mounting with the clamps were used to make the test bench demountable, and therefore as mobile as possible. The S-load cells allowed to measure the force of the proband during MVC. The signal of the S-Load cells was amplified with a gain of 1000 by an instrumentation amplifier INA 114AP and afterwards A/D converted by an Arduino micro, which also supplied the S-Load cells with a 5V voltage. The instrumentation amplifier was supplied with two 9V batteries. A schematic of the measurement circuit can be seen in Figure 29.

The program for the Arduino micro was written in Arduino IDE (Arduino SRL, Torino, Italy). If a trigger-signal arrived from the NI 6001 (by starting the EMG acquisition), the Arduino started to record the voltage values from the two S-load cells. The values were transmitted serially, until another trigger-signal was sent. The serial values were imported with a Matlab (Mathworks Inc., Natick, USA) program for further processing. The imported matrix was split up in two vectors, one for each load cell. An

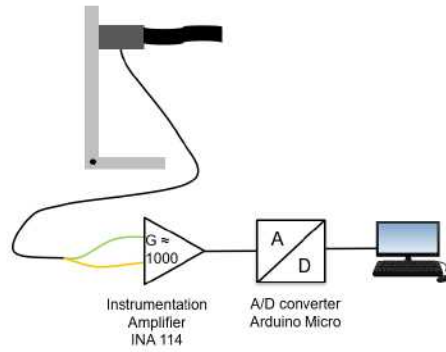


Figure 29: Schematic of the testbench

offset correction was done, the ADC values were converted to kg by the evaluated formula (4) below and then the forces of the two cells were added. The force was multiplied by the distance between hinge and load cells (285mm), so the output was a torque over time curve in Nm.

To calibrate the test bench the upper board was mounted on a table with the two clamps (figure 30). Three different weights were hung on the belt as seen in figure 30. With every weight five measurements were done.



Figure 30: Setup for the verification of the mobile test bench

A mean value of these five measurements was calculated. With these mean values a relation between the force, produced by the hung up weight, and the ADC value was created (see table 4 and figure 31).

Table 4: Average ADC value to force relation

Force in kg	ØADC-readout
0	0
5	37,6804
8	62,688
13	100,1087



Figure 31: Relation between the average of the measured ADC value and the force, produced by the hung up weight

The relation, calculated using the function "trend line" in Excel (Microsoft Corporation, Redmond, USA) is:

$$Force \ in \ kg = \frac{\text{Ø ADCvalue} + 0,5225}{7,7709} \quad (4)$$

## 5.2 Verification of Hardware and Signals

### 5.2.1 Ultrasound-Transparent Material

For the verification of the US transparent material the setup in Figure 32 was used.

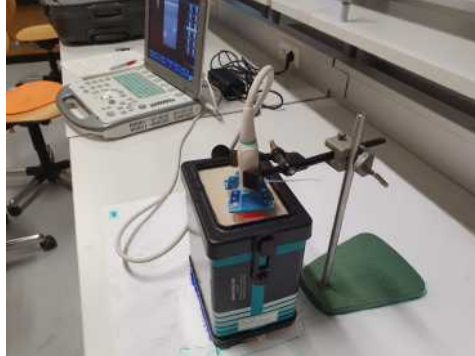


Figure 32: Setup for the verification of the US-transparent material

A CIRS US phantom was filled with water and US images were captured in a repeatable manner. In the first session, US images without the EMG-adapter were recorded, in session two the EMG-adapter was fixed on the US transducer. To image the same defined position in every session a fixture was used to position the transducer. The position of the fixture and the CIRS phantom was marked. Because of the use of water no US-gel was necessary, so there were the exact same conditions in session one and two. In every session five images were recorded. A mean value of these images was built and histogram curves of 1D lines in five different depths were calculated. The location of these 1D lines are sketched in figure 33. Above the blue line, the EMG layer is visible.

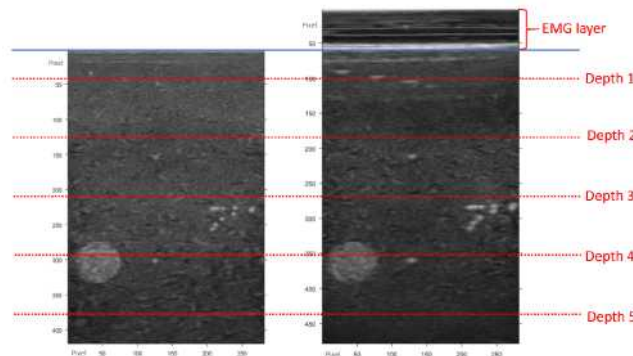


Figure 33: Left side: US image of session one, recorded without EMG-adapter. Right side: US image of session two, recorded with the EMG-adapter. The red, dashed lines mark the five depths, used to calculate the histogram curves.

The images of the two sessions were compared using histogram curves. Calculation and comparison were done in Matlab (Mathworks Inc., Natick, USA).

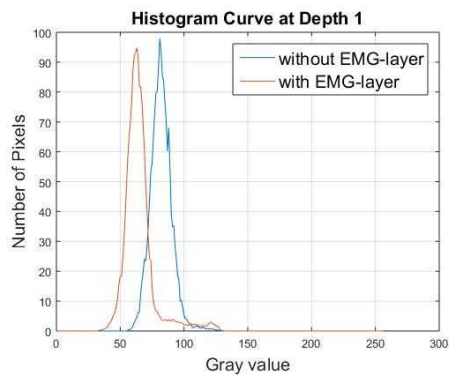


Figure 34: Histogram at depth 1

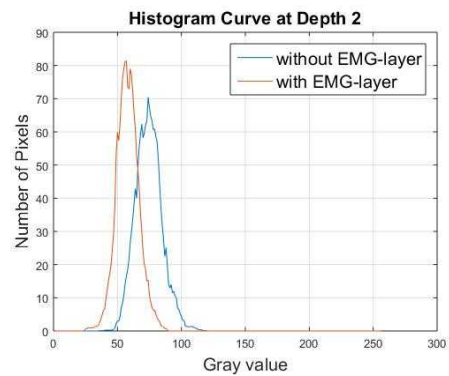


Figure 35: Histogram at depth 2

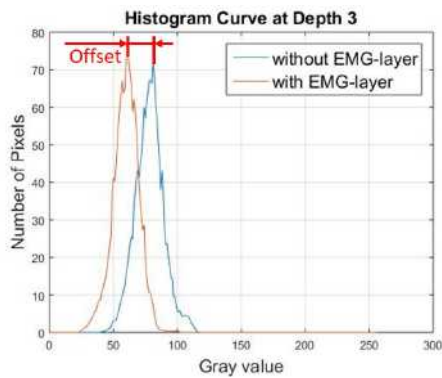


Figure 36: Histogram at depth 3

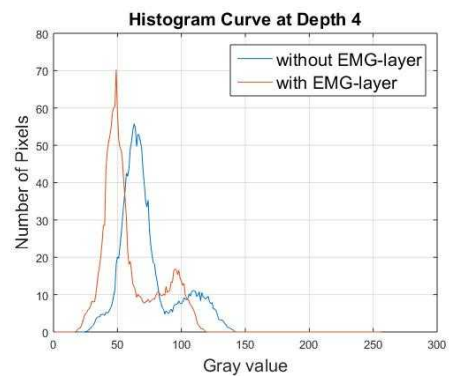


Figure 37: Histogram at depth 4

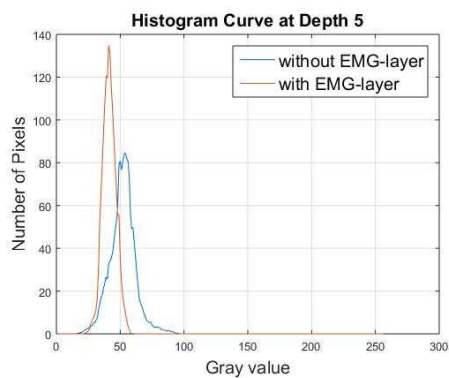


Figure 38: Histogram at depth 5

Figures 34 - 38 show the results for the different image depths. The blue curves show the histogram curves from the image with the EMG adapter. The orange ones show the

histogram curves from the image, recorded without the EMG adapter. A mean offset of about 17 gray values is visible. This offset was marked as an example in figure 36 for depth 3. The course of the two curves in each depth is almost the same. This indicates that the recorded image gets darker due to the US transparent layer, but there is almost no quality loss. Only the 17 darkest gray tones are lost because they are all displayed as black.

### 5.2.2 Biosignal Verification of the US Transparent EMG Electrode

To verify the biosignals recorded by the self-made EMG-sensors, EMG signals during an isometric, maximum voluntary contractions of a human biceps brachii were recorded with one channel of the developed US- transparent EMG electrode and compared with signals, recorded with adhesive electrodes on the same setup. The positioning of the electrodes can be seen in figure 39 (selfmade electrode) and figure 40 (adhesive electrodes).

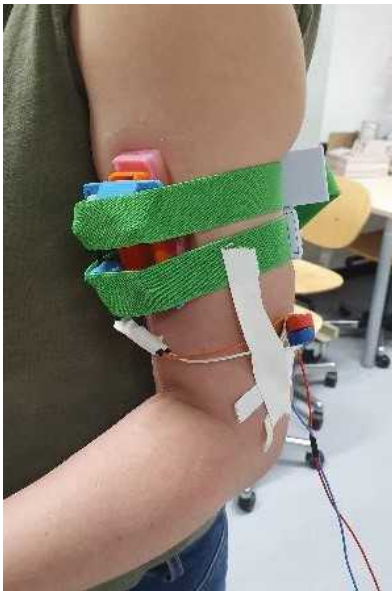


Figure 39: Electrode positioning of the US-transparent EMG-electrode for the biosignal verification



Figure 40: Electrode positioning of the adhesive EMG-electrode for the biosignal verification

The smallest possible IED with the adhesive electrodes was 2cm. The ground electrode was fixed on the wrist. For the force generation the proband had to stand upright, keep his left hand in a right angle next to his body and pull as hard as possible on a strap, which he held against with his left foot.

With both electrodes ten signals were recorded via the developed EMG acquisition device and then offset corrected, rectified, smoothed and standardized with a Matlab (Mathworks Inc., Natick, USA) program (see chapter 4.4.2 way three).

Furthermore statistical parametric mapping was done to evaluate the results. The two

sample T-Test was chosen, because the two tests were independent. In figure 41 the results of the two sample T-test can be seen. The bold lines are the means of ten signals per session. The red one is from the signals, recorded by the US-transparent EMG electrode, the black one from the adhesive electrodes. Their standard deviations are marked as a cloud in the same colors, respectively. On the right side the two curves get compared by a hypothesis test. A  $\alpha$  of 0.5 was used. The critical t-value  $t^*$  is calculated to 4.7326. The red dashed lines in figure 41 (right) mark this value. The black curve shows the t-values for every time step. The two recorded configurations were tested against the null-hypothesis and did not reveal significant differences.

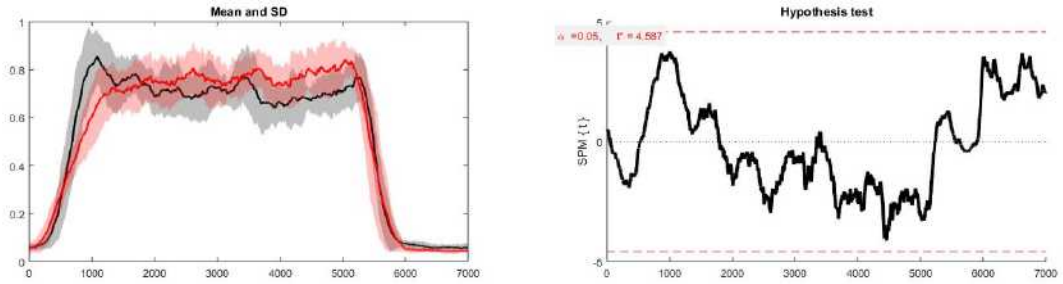


Figure 41: Left side: Mean and standard deviation of ten signals per session. Red session: US- transparent EMG electrode, black session: adhesive electrodes. Right side: Hypothesis test.

It was not possible to reach the same IED and electrode diameter with the adhesive electrodes and the US transparent electrodes, therefore slight but insignificant differences between the two measurements exist. Furthermore, adhesive electrodes were only available with a diameter of 10mm and the smallest possible IED, so that they still stick and contact the skin, was 20mm. The developed US transparent electrodes had a diameter of 4mm and an IED of 8mm.

### 5.2.3 EMG Acquisition Device

For this process, the EMG of a human biceps brachii during an isometric maximum voluntary contraction was measured. Two adhesive electrodes were mounted on the biceps, one ground electrode on the wrist. The same setup for force generation as in chapter 5.2.2 was used. The whole setup can be seen in figure 42, left side.

The electrodes were connected to the self-made EMG measurement circuit (figure 42, bottom right) and to the biowolf system (figure 42, top right) at the same time. So it was possible to record the same EMG signals with both devices simultaneously. The biowolf system is a sub-10-mW 8-channel advanced brain-computer interface platform with a nine-core processor and BLE connectivity [35]. Ten measurements were done. The two devices were compared again via a two sample T-test in Matlab (Mathworks

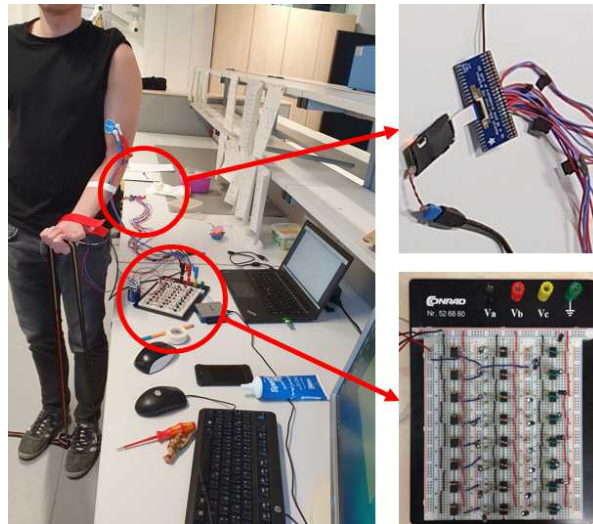


Figure 42: Setup for the Verification of the Developed EMG Acquisition Device. Top right: biowolf-system. Bottom right: Developed EMG Acquisition Device

Inc.,Natick, USA). The same program as in chapter 5.2.2 was used (see chapter 4.4.2, way three).

Figure 43 shows the results of the two sample T-test.  $\alpha$  was again set to 0,05. The red bold line is the mean value of the ten signals, recorded with the developed EMG. The red cloud is the standard deviation of them. The black part is the same from the biowolf signals. On the right side the hypothesis test is visible. Again, the t-values (black curve) at every time-step is within the  $t^*$  limits (red dashed lines). In this case, the critical t-value  $t^*$  was calculated to 4.733. The result is that the two samples do not reveal significant differences.

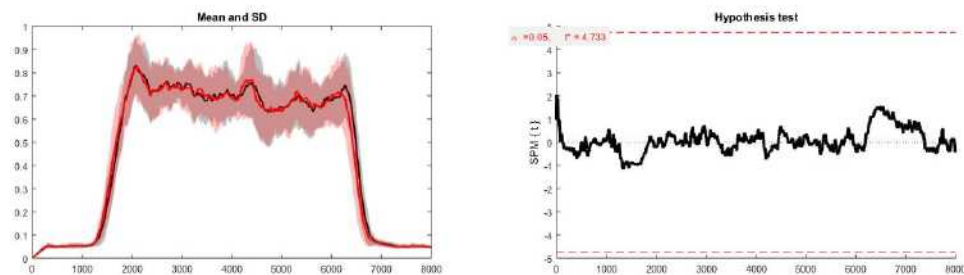


Figure 43: Left side: Mean and standard deviation of ten signals per session. Red session: EMG recorded with biowolf, black session: EMG recorded with developed EMG. Right side: Hypothesis test.

Nearly no variation between both setups was observed.

### 5.2.4 Mobile Test Bench

In figure 44, the force of a proband during an isometric plantarflexion in Nm is shown. The curve is recorded on the mobile test bench. A maximal force of about 100 Nm was reached.

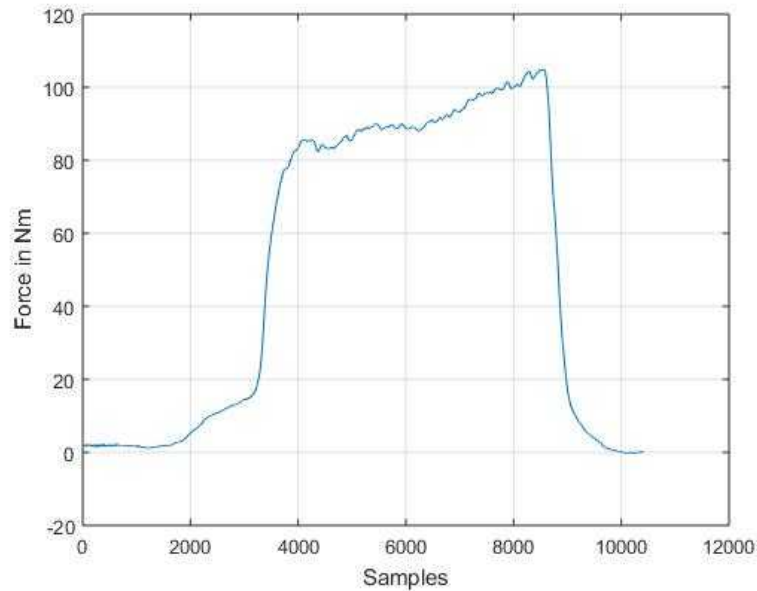


Figure 44: Force in Nm, measured during MVC on MG

This torque-curve shows plausible values, as reported in literature. Reference values are  $169.4 \pm 52.9$  Nm [36], and  $132 \pm 20$  Nm [37], depending on sex, age and physique of the probands. Hence, this confirms the validity of the test bench.

The measured value is in the lower range in both researched spectra. The reason is maybe that the measurement was repeated very often and the muscle was fatigued.

## 5.3 Measurement of Human Muscle Contractions In Vivo

In this chapter the developed setup was applied on a human proband. Measurements on biceps brachii were done to show synchronized US images and HDsEMG signals. The biceps brachii was chosen because of its parallel muscle fibers, to show MUAPs in HDsEMG signals. Measurements on medial gastrocnemius were done to include measurement of force exertion and to show synchronized US, HDsEMG and force recording.

### 5.3.1 Measurements on Biceps Brachii

Fifteen parallel US and EMG investigations were recorded. To generate a MVC, the same setup as in chapter 5.2.2 was used. The arrangement of the channels on the biceps can be found in figure 45.

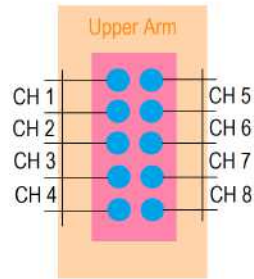


Figure 45: Arrangement of EMG channels during investigation of biceps brachii

In figure 46 an overview of a parallel US-HDsEMG investigation of biceps brachii is visible. On the upper part of the figure the EMG signals of the eight channels are shown. On the bottom the US images of the muscle, one time relaxed and one time during MVC, can be seen. The layer of the EMG electrode, the skin and fat layer and the muscle tissue can be recognized. The white, parallel lines show the muscle fiber bundles. The muscle fiber direction was visualized with the help of the yellow line.

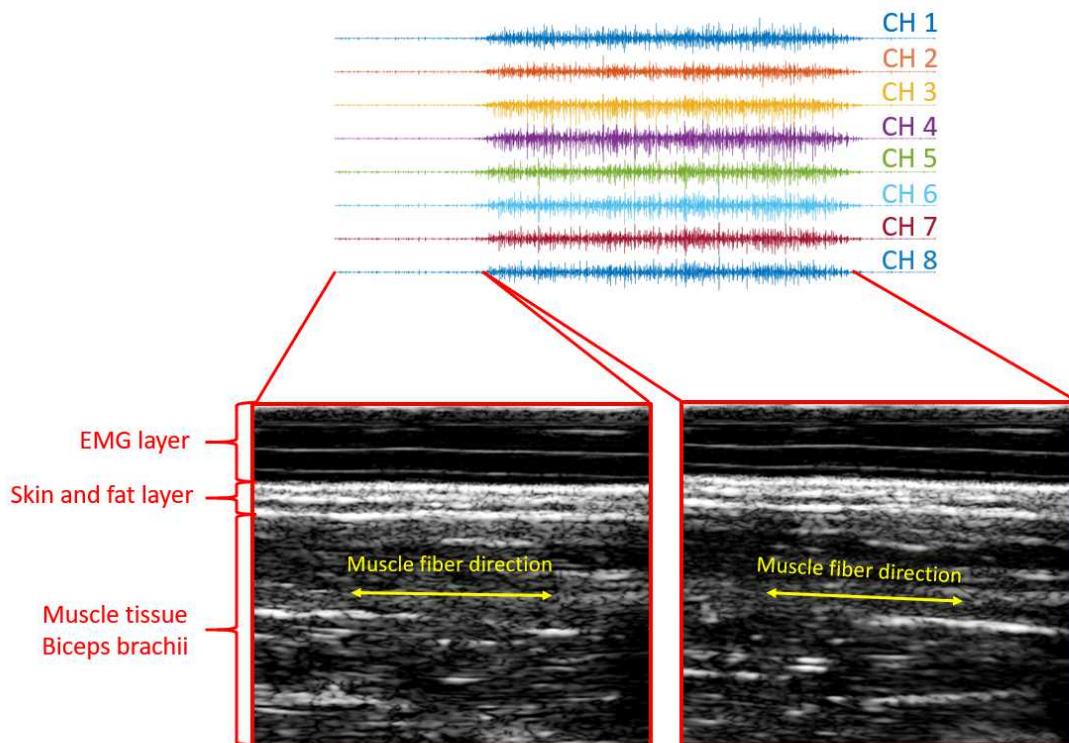


Figure 46: Parallel US and EMG acquisition. At the top: EMG signal of the eight channels. At the bottom, left: US image of biceps brachii during relaxation and right during MVC.

This muscle was chosen, because there is only a very thin layer of fat and skin between its muscle tissue and the body surface. In addition, the muscle fibers run nearly parallel along the arm. Comparing the two US images in figure 46 (on the left side, relaxed muscle, on the right side, muscle during contraction), it can be seen that the muscle fiber direction almost doesn't change during muscle contraction.

To make the frequency spectrum of the recorded EMG signals visible, a fast Fourier transformation of each channel-signal was performed (see figure 47). It can be seen that the main components of the recorded signals are situated between about 50 Hz and 200 Hz. The mean frequencies (red lines in figure 47) are about 100 Hz to 150 Hz. The median frequencies (green lines in figure 47) vary between 100 Hz and 130 Hz.

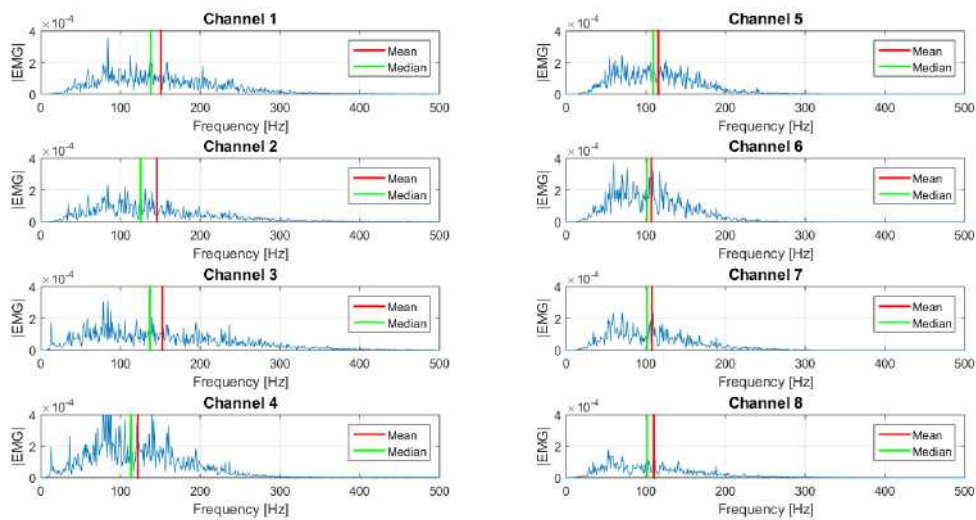


Figure 47: Frequency spectrum of the EMG signals, recorded on biceps brachii

The frequency spectrum of the recorded signal fits exactly the expected frequency spectrum from about 15Hz to 400Hz [26], which emerges from the literature research (see chapter 2.3).

To check whether a signal of a channel is valid, a CCA was done. If the CCA signal is in the size of the EMG signal itself, the signal is very noisy and not valid, because the change of the signal between one sample to the next sample is very high. If the CCA signal is very small in comparison to the EMG signal, the channel is valid. This check was done with each channel at each acquisition. In figure 48, the EMG signals incl. CCA of all eight channels during a MVC are illustrated. The band pass filtered EMG signals are represented by the blue curves. The orange curves are the curves after CCA of each channel. It can be seen that channels 1 to 4 are very noisy and thus useless for detailed observation. However, onset and offset of the signals can still be seen. Channels 5 to 8,

the right row seen from above, are valid and are therefore used for further inspection.

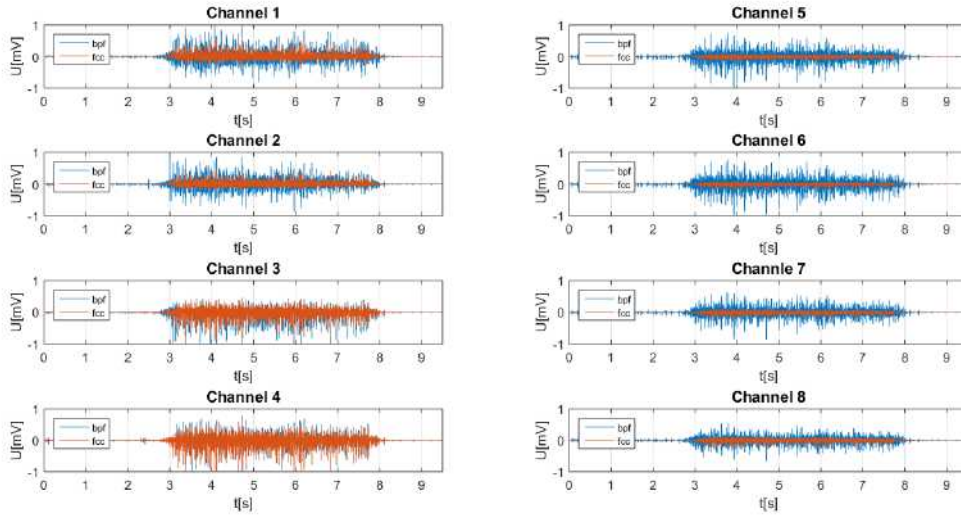


Figure 48: Overview of the 8 HDsEMG signals of biceps brachii during MVC. Blue: HDsEMG signal. Orange: Same signal after Common CoSDonent Analysis.

The reason for the noise at channels 1 to 4 could be the electrode skin resistance, which is maybe different at the two rows, because the pressure is not evenly distributed over the whole electrode.

With figure 49 a detailed visual inspection of the HDsEMG signals was done after zooming into the signals. The blue curves are the EMG signals after band pass filtering, the green ones are the signals after CCA. On the left side the channel number is visible. The signals are normalized to the global maximum.

Carrying out a detailed inspection of this EMG signals, it can be seen that it was possible to record a MUAP. This assumption is confirmed by several facts. First, the shape of the curve in figure 49, for example at channel 5 between sample 3372 and sample 3386, matches that of a MUAP (see figure 7). The next fact is that the MUAP moves with a velocity of approximately 4m/s. This can also be observed in figure 49. The red dashed line marks the peak of every MUAP at every channel. The peak moves from one channel to the next, so 8 mm, in 2 samples. Since the sampling frequency  $f_s$  is 1000 Hz, this can be transformed to a velocity of 4 m/s. This is exactly the propagation velocity of APs, which resulted from the literature research [19] in chapter 2.1.3. In addition, as mentioned before, the signal is in the correct frequency spectrum and not noisy.

The average wave propagation velocity for channel 5 to 8, calculated in Matlab, was 4.1155 m/s, with a cross-correlation coefficient of 0.8575. This cross-correlation coefficient confirms the similarity of the time-shifted signals of channels 4 to 8. The cross-correlation coefficient in general can be between -1 and 1. The closer it is to 1, the more

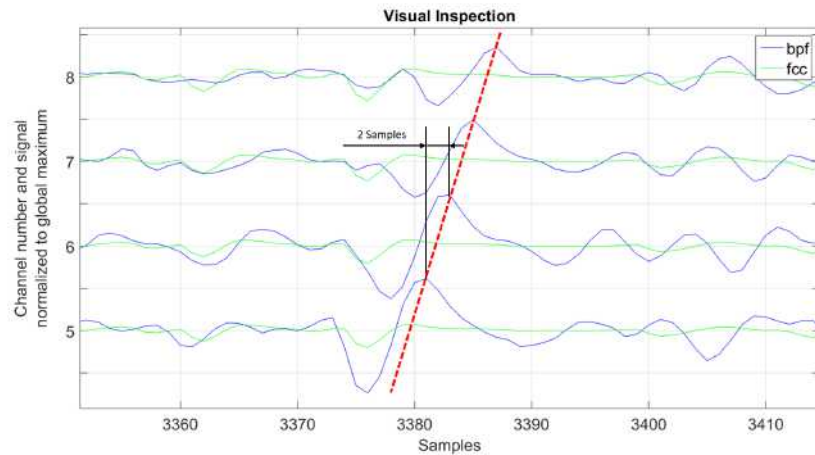


Figure 49: Zoomed in HDsEMG signal of all eight channels, recorded on biceps brachii

similar the signals are.

In figure 49, it is also visible that the IZ is located closer to channel 5 as to channel 8. This is because the MUAP propagates towards channel 8.

Looking at these facts, it can be detected that the EMG signals, recorded by the developed system, are valid.

### 5.3.2 Measurement on Medial Gastrocnemius

To investigate the medial gastrocnemius the proband was fixed in the test bench and fifteen parallel US-HDsEMG recordings were done. The same channel arrangement as in figure 45 was used. In addition, the torque during the MVC was measured in Nm. Figure 50 illustrates the whole setup.

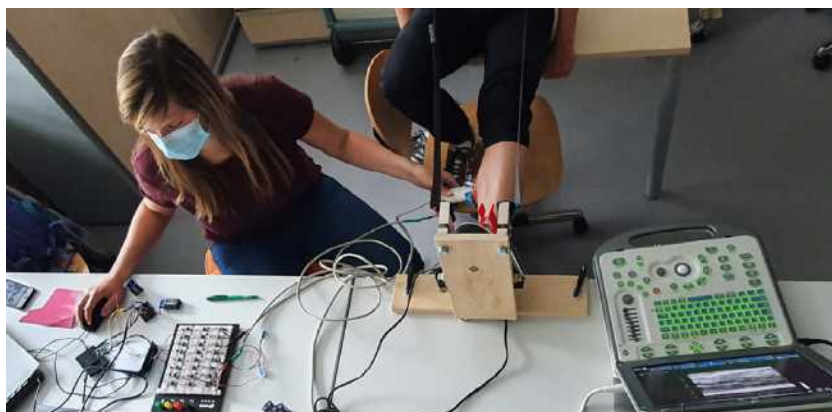


Figure 50: Investigation of the behaviour of medial gastrocnemius during a MVC

Figure 51 shows an overview of the parallel US-HDsEMG investigation of a human medial gastrocnemius. On the top, the signals of the eight HDsEMG channels, are shown. On the bottom left, an US image of the relaxed MG during EMG recording can be seen. On the right side the MG during MVC is visible. Again, the layer of the EMG electrode, the skin and fat layer and the muscle tissue together with the muscle fiber direction can be recognized. The upper muscle tissue is the medial gastrocnemius. The tissue on the lower side is the soleus tissue.

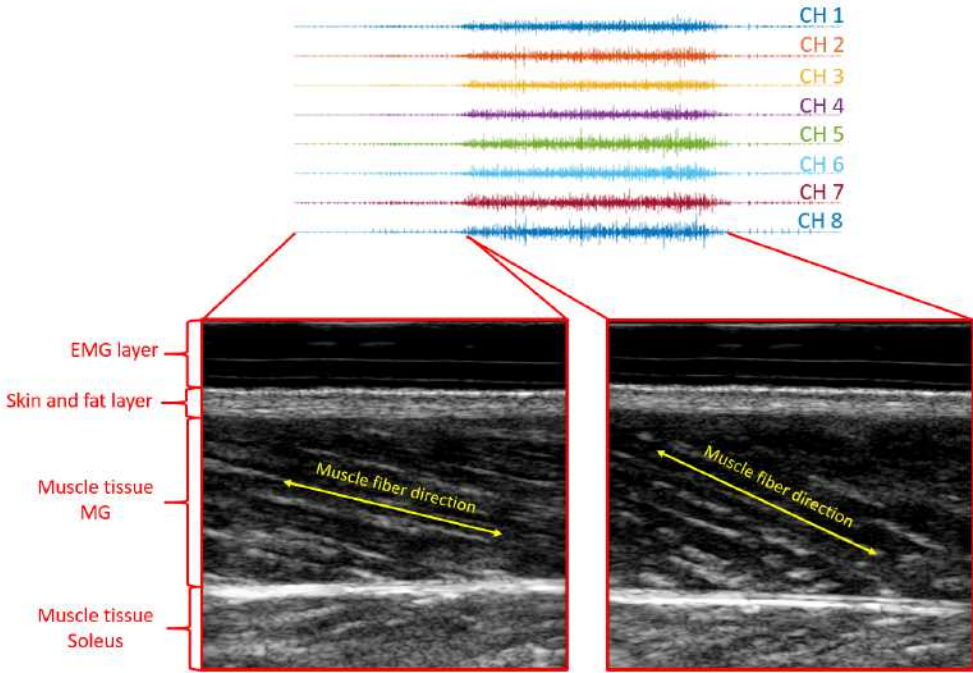


Figure 51: Parallel US and EMG acquisition. At the top: EMG signal of the eight channels. At the bottom, left: US image of medial gastrocnemius during relaxation and right during MVC.

It can be seen that the muscle fibers of the MG are situated at an angle to the long axis of the muscle. This type of muscle is called pennate muscle (see chapter 2.1.1).

In order to check the correctness of the recorded EMG signals, as well as the noise components of the recorded EMG signals, again signal processing as described in 4.4.2 was done. A FFT (signal processing way one, see figure 52) and a CCA (signal processing way two, see figure 53) were performed.

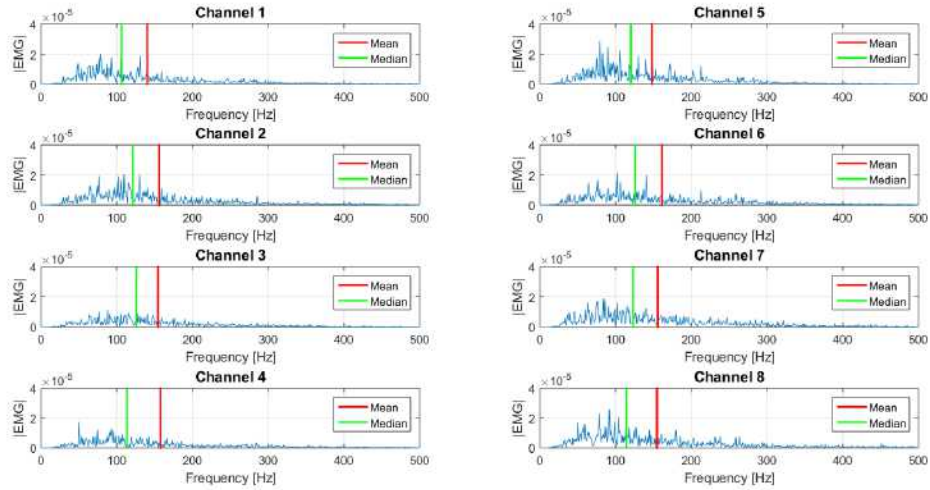


Figure 52: Frequency range of HDsEMG signals, recorded on MG during MVC. Red: Mean frequency. Green: Median frequency.

Again, it is visible, that the main components of the recorded signals are situated between about 50 Hz and 200 Hz what is the expected spectrum. The mean frequencies (red lines in figure 52) are about 100 Hz to 130 Hz. The median frequencies (green lines in figure 47) vary between 140 Hz and 160 Hz.

In figure 53 the band pass filtered EMG signals are illustrated in blue and the signals after CCA are shown in orange.

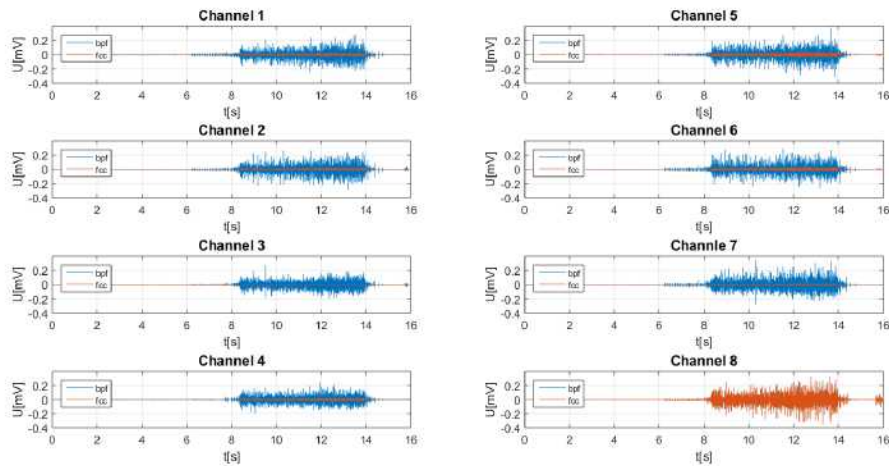


Figure 53: Blue: HDsEMG signal of a MVC, recorded on MG after band pass filtering. Orange: Same signal after a Common CoSDonent Analysis.

It can be seen that channel 8 is very noisy and therefore useless. During measurements it could be detected that channel 8 was often very noisy. That is probably because channel 8 was located on the edge of the electrode. There the pressure on the electrode could have been a little different. As a result the electrode skin resistance was too high. However, the noise could have been caused by poor skin preparation or cable movement, too.

For detailed inspection a zoom into signals of channel 1 to 4 was done. This is visible in figure 54. The blue signal is the EMG signal after band pass filtering, the green one is the CCA signal.

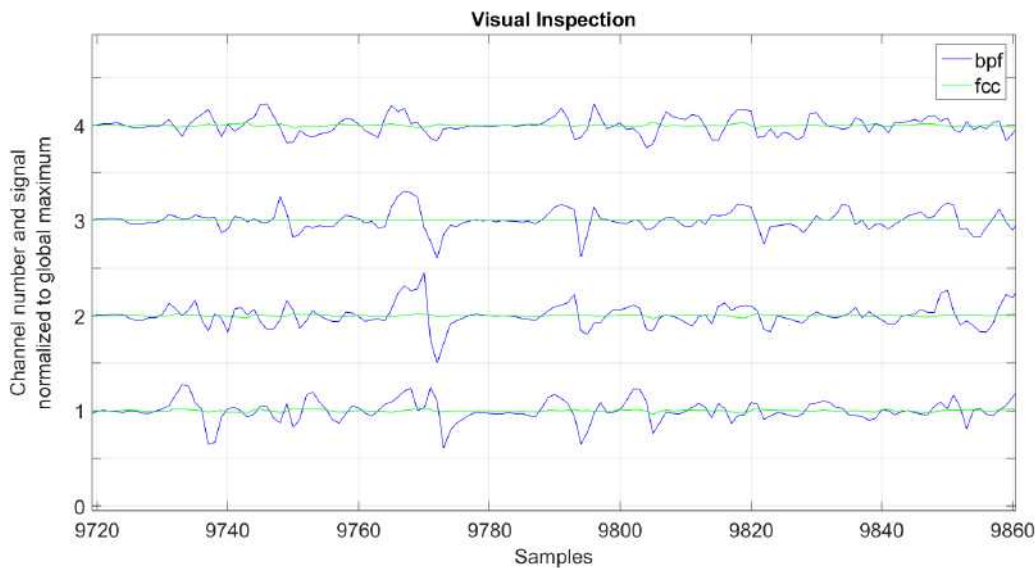


Figure 54: Zoomed in HDsEMG signal (blue) of channel 1 to 4 during MVC, measured on MG. Green: CCA

Although the correctness of the signals is confirmed, it is not possible to see a MUAP at a detailed visual inspection in figure 54. The reason for that is the arrangement of the muscle fibers. As mentioned in chapter 2.1.1 and seen in figure 51, is the medial gastrocnemius a pennate muscle, so its muscle fibers are arranged at an angle and not parallel to the long axis as at biceps brachii. Since the AP starts at the MEP and propagates toward the fiber end in both fiber directions similar but inverted, the APs of the individual parallel muscle fibers at biceps brachii add up (represented by the green arrows in figure 55) and one "total" AP can be measured by the acquisition device, because the electrode is arranged parallel to the muscle fibers.

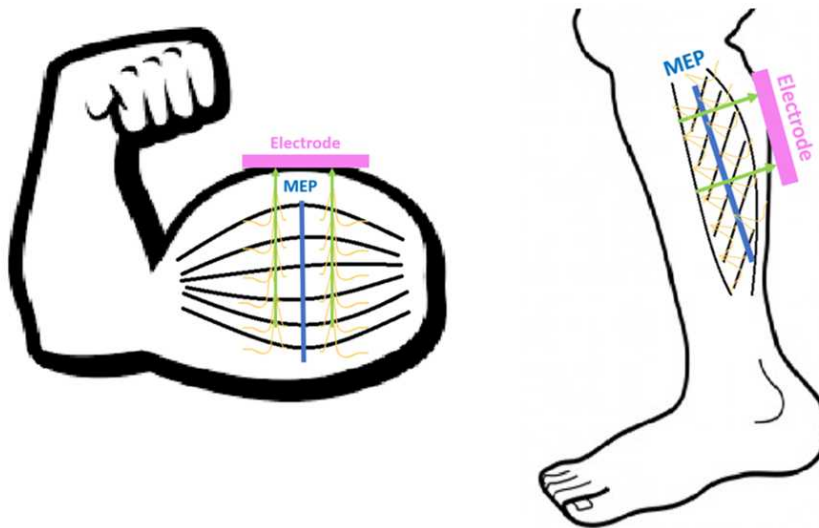


Figure 55: Muscle fiber arrangement of biceps brachii (left) and medial gastrocnemius (right)

The APs at medial gastrocnemius do not take place parallel one above the other, seen from the electrodes position, because it is not possible to place the electrode parallel to the muscle fibers. Different parts of the APs are added up and these results are the curves in figure 54.

In figure 56, the correlation between EMG signals and the measured muscle force is visible. All signals are displayed in [%] normalized to their global maximum.

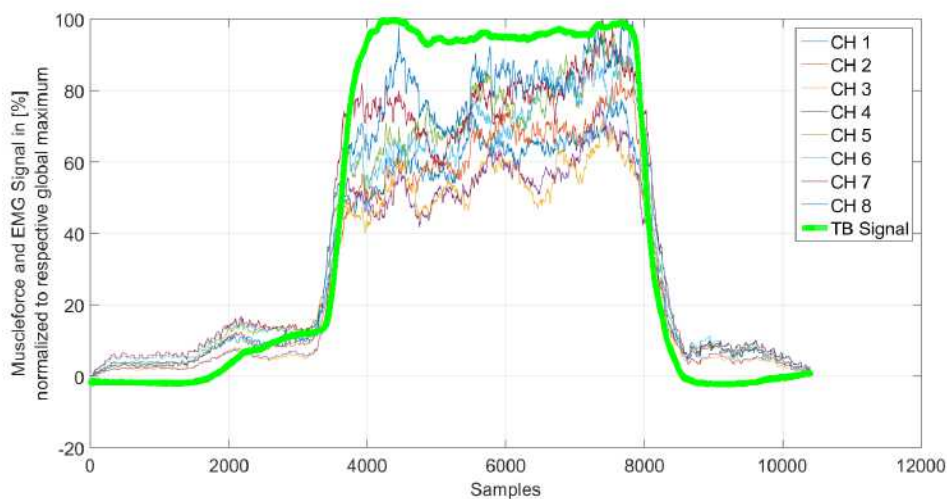


Figure 56: Green: Normalized torque, measured on TB during MVC. Others: HDsEMG signals standardized to muscle force

It is possible to observe a general correlation between the measured torque and the EMG signal. The on- and offset of the torque signal matches with the on- and offset of the EMG signals. However, a clear linear behaviour could not be identified and needs to be further investigated in future works.

## 5.4 Discussion

In conclusion, this thesis shows the development of a functional low-cost laboratory setup to record muscle properties (length changes and activation) during contractions using ultrasound and an ultrasound transparent high density electrode grid. The resolution of the EMG signals and the US images were comparable with literature. MUAPs were able to be detected. Nevertheless some limitations need to be discussed.

First, due to the length of the cables between the electrode-connectors and the acquisition device some noise was coupled in. Despite the shielded design the noise was caused because of cable moving. To reduce this the cables were fixed with tape onto the proband. One possible solution for the future would be to place the acquisition device very close to the electrodes.

Secondly, because the EMG sensors were made of copper wire braids, the different electrode-skin resistances on every sensor were another problem during signal recording. The advantage of these thin wires was that they were nearly not visible in US images. But it was not possible to get the exactly same braid in the exactly same position for every sensor. To get a better contact, electrode gel was used. The problem here was, that it was very difficult to keep the gel inside the small wholes. If the gel leaked from the wholes, it was possible that it caused a short between two electrodes. To fix these problems, sensors with a fix size, made of, for example, Ag/AgCl should be used in the future. To reduce the influence of the high electrode-skin resistances, an input amplifier (INA 114 AP) with an extremely high input impedance of approximately  $10^{10} \Omega$  was used. A high input impedance reduces the input current, and so the voltage drop on the sensor impedance.

The surface of the human body and cables are constantly exposed to electromagnetic radiation and act like antennas for ambient noise, like the 50 Hz supply frequency and their harmonics, starting on, for example, electrical devices in the environment. Since 50 Hz signals are essential parts of the human EMG signal, it is not possible to filter them without any loss of information. Therefore, the bipolar method was used. The two signals are subtracted from each other and the resulting differences are amplified. Signals from more distant sources, brought in from different antennas, arrive almost at the same time at the two electrodes and are therefore mostly canceled out. Nevertheless, care was taken that electrical equipment was placed as far away as possible. In addition the input amplifier had a high common mode rejection ratio (CMRR), which means, that the change of the output voltage is very small, if a signal appears simultaneously and in-phase on both inputs. The EMG acquisition device and the mobile test were

supplied with 9V batteries to avoid the risk of an electric shock in case of a failure.

Finally thin silicon layers are more beneficial for better US images. However due to the wiring and casting methods layer thickness cannot be reduced infinitely and have a limit of approx. 2 mm in the current setup.

Despite its simple and low-cost structure, it has been demonstrated that the US transparent EMG achieved reliable and repeatable signals across different muscles and activations.

## 6 Conclusion

The scope of this thesis was to record ultrasound images and high density surface electromyograms of a human extremity in synchronized mode. The advantage of this parallel investigation is that it is possible to record the grade of activation, the muscle length and the rate at which the muscle changes its length, so the three values on that the muscle force mainly depends, during one investigation.

A low-cost, mobile test bench to investigate muscle behaviour during an isometric maximum voluntary contraction, using a combination of high-density surface EMG and ultrasound, was designed. The setup was verified and validated, using statistical methods and measurements on a human proband were carried out. It was possible to reach comparable results with literature. Ultrasound images with only slightly impaired quality were recorded during HDsEMG. The signals recorded by EMG acquisition device and EMG electrodes showed no significant difference between signals recorded by common available devices. Even individual MUAPs were able to be detected by the ultrasound transparent HDsEMG. The developed test bench was mobile and it was possible to record the torque during isometric plantarflexion, triggered with the EMG acquisition, in defined and repeatable conditions.

In further works, the quality of the EMG signal could be improved by using a different electrode material and shape. The quality of the ultrasound image could be increased by a thinner layer of silicone or by a different US transparent material between skin and US transducer. Moreover, a reduction of cables could reduce noise. This could be achieved by minimizing the EMG acquisition device and placing it right next to the electrode.

In conclusion, this thesis describes a low-cost and mobile test bench to collect muscle activation data by HDsEMG and muscle length data by ultrasound in synchronized mode.

## References

- [1] TechTarget, <https://whatis.techtarget.com/definition/locomotion>, 2020-04-30.
- [2] Paavo V Komi. Stretch-shortening cycle: a powerful model to study normal and fatigued muscle. *Journal of Biomechanics*, 33:1197–1206, 2000.
- [3] Eadweard Muybridge. *Animal Locomotion*. Springer, 1887.
- [4] N. A Bernstein. *The co-ordination and regulation of movements*. Science, vol. 159 edition, 1968.
- [5] H. Huxley and J. Hanson. Changes in the Cross-Striations of Muscle during Contraction and Stretch and their Structural Interpretation. *Nature*, 173:973–976, 1954.
- [6] A.V. Hill. The heat of shortening and the dynamic constants of muscle. *Proceedings of the Royal Society of London. Series B - Biological Sciences*, 126(843):136–195, 1938.
- [7] Thomas J Roberts and Annette M Gabaldón. Interpreting muscle function from EMG: lessons learned from direct measurements of muscle force. *Integrative and comparative biology*, 48:312–320, 2008.
- [8] B. Frenzel-Beyme. Ultraschallmuseum, [https://www.ultraschallmuseum.de /index.php?link=120](https://www.ultraschallmuseum.de/index.php?link=120), 2020-10-08.
- [9] F. Buchthal, P. Pinelli, and P. Rosenfalck. Action Potential Parameters in Normal Human Muscle and their Physiological Determinants. *Acta Physiologica Scandinavica*, (32(2-3)):219 – 229, 1954.
- [10] Armin Curt and Uta Kliesch. *Neurophysiological Investigations*. Springer, Berlin, Heidelberg, 2008.
- [11] Christoph Leitner, Christian Baumgartner, Simone Benatti, Brigitte Schober, and Christian Peham. A Non-Invasive , Multimodal Method to Investigate Muscle Functions in Hind Limbs of Canine. 2020.
- [12] Rice University. *OpenStax, Anatomy & Physiology*. Rice University, 2016.
- [13] Christoph Leitner, Sergei Vostrikov, Markus Tilp, Pascal A. Hager, Andrea Cossettini, Luca Benini, and Christian Baumgartner. Human fascicle strain behavior during twitch using ultrafast ultrasound. *2020 IEEE International Ultrasonics Symposium (IUS)*, 2020.
- [14] Bruce M. Carlson. *The Human Body*. 2017.
- [15] Roberto Merletti and Dario Farina. *Surface Electromyography: Physiology, Engineering and Applications*. Wiley-IEEE Press, apr 2016.

- [16] Peter Konrad. EMG-FIBEL- Eine praxisorientierte Einführung in die kinesiologische Elektromyographie. 2011.
- [17] Franz Gerrer, <https://www.medizin-kompakt.de/>, 2020-06-04. Medizin-Kompakt.de.
- [18] F. Buchthal and H. Schmalbruch. Motor unit of mammalian muscle. *Physiological Reviews*, 60:90–142, 1980.
- [19] R. Merletti and S. Muceli. Tutorial. Surface EMG detection in space and time: Best practices. *Journal of Electromyography and Kinesiology*, 49, 2019.
- [20] Karin Roeleveld, Joleen H. Blok, Dick F. Stegeman, and Adriaan Van Oosterom. Volume conduction models for surface EMG; confrontation with measurements. *Journal of Electromyography and Kinesiology*, 7:221–232, 1997.
- [21] I. D. Loram, C. N. Maganaris, and M. Lakie. Use of ultrasound to make noninvasive in vivo measurement of continuous changes in human muscle contractile length. *Journal of Applied Physiology*, vol 100:1311–1323.
- [22] Francis Walker and Michael Cartwright S. *Neuromuscular Ultrasound*. 2011.
- [23] Pascal Alexander Hager. *Design of Fully-Digital Medical Ultrasound Imaging Systems*. PhD thesis, 2019.
- [24] Carol M. Rumack and Deborah Levine. *Diagnostic Ultrasound*, volume 19. Elsevier Inc., 2018.
- [25] Andrew Murphy and Matt A. Morgan. Acoustic impedance.
- [26] M.A. Cavalcanti Garcia and T.M. M. Vieira. Surface electromyography: Why, when and how to use it. *Medicina del Deporte*, 43:176, 2019.
- [27] Surface electromyography for noninvasive characterization of muscle. *Exercise and Sport Sciences Reviews*, 29(1):20–25, 2001.
- [28] Holger Urbanek and Patrick van der Smagt. iEMG: Imaging electromyography. *Journal of Electromyography and Kinesiology*, 27, 2016.
- [29] Guzmán Rodrigo A., Silvestre Rony A., and Arriagada David A. Biceps Brachii Muscle Innervation Zone Location in Healthy Subjects Using High-Density Surface Electromyography. 29(2):347–352, 2011.
- [30] Xin Chen, Yong Ping Zheng, Jing Yi Guo, Zhenyu Zhu, Shing Chow Chan, and Zhiguo Zhang. Sonomyographic responses during voluntary isometric ramp contraction of the human rectus femoris muscle. *European Journal of Applied Physiology*, 112(7):2603–2614, 2012.

- [31] A Botter, T M M Vieira, I D Loram, R Merletti, and E F Hodson-Tole. A novel system of electrodes transparent to ultrasound for simultaneous detection of myoelectric activity and B-mode ultrasound images of skeletal muscles. *Journal of applied physiology (Bethesda, Md. : 1985)*, 115:1203–14, 2013.
- [32] A. Botter, M. Beltrandi, G.L. Cerone, M. Gazzoni, and T.M. Vieira. Development and testing of acoustically-matched hydrogel-based electrodes for simultaneous EMG-ultrasound detection. *Medical Engineering and Physics*, 64:74–79, 2019.
- [33] Manfred Albach. *Elektrotechnik*. Pearson Deutschland GmbH, 2011.
- [34] Todd C Pataky. Generalized n-dimensional biomechanical field analysis using statistical parametric mapping. *Journal of biomechanics*, 43(10):1976–1982, 2010.
- [35] V. Kartsch, G. Tagliavini, M. Guermandi, S. Benatti, D. Rossi, and L. Benini. Biowolf: A sub-10-mw 8-channel advanced brain–computer interface platform with a nine-core processor and ble connectivity. *IEEE Transactions on Biomedical Circuits and Systems*, 13(5):893–906, 2019.
- [36] Josh R. Baxter and Stephen J. Piazza. Plantar flexor moment arm and muscle volume predict torque-generating capacity in young men. *Journal of Applied Physiology*, 116(5):538–544, 2014.
- [37] Jens Bojsen-Møller, Philip Hansen, Per Aagaard, Ulla Svantesson, Michael Kjaer, and S. Peter Magnusson. Differential displacement of the human soleus and medial gastrocnemius aponeuroses during isometric plantar flexor contractions in vivo. *Journal of Applied Physiology*, 97(5):1908–1914, 2004.

# List of Figures

1	Eadweard Muybridge, photographic movement studies of a horseman and his horse [3] . . . . .	6
2	Muscle model by A. V. Hill, 1938 [6] . . . . .	7
3	Structure of a skeletal muscle [12] . . . . .	9
4	Schematic representation of a sarcomere during relaxation and contraction [5] . . . . .	10
5	Types of internal architectures in muscles . . . . .	11
6	Flow of sodium and potassium during depolarization and repolarization of a muscle cell. Modified from [16] . . . . .	12
7	Action potential [12] . . . . .	12
8	Propagating of an AP over a muscle fiber. Modified from [20] . . . . .	13
9	B-Mode US . . . . .	16
10	1) and 2) Monopolar detection method 3) Bipolar detection method . . . . .	17
11	Electrode array for HDsEMG . . . . .	18
12	Anterior shoulder and arm with biceps brachii . . . . .	21
13	Lower leg with gastrocnemius . . . . .	22
14	CIRS General Purpose Ultrasound Phantom Model 054GS . . . . .	22
15	Ultrasound equipment Mindray M5 . . . . .	23
16	Schematic of INA 114AP . . . . .	24
17	Load cell from PSD . . . . .	25
18	Arduino Micro . . . . .	25
19	Signal processing for ultrasound images . . . . .	26
20	Three ways of signal processing for HDsEMG signals . . . . .	26
21	Left side: Previous solutions of US transparent EMG electrodes. Right side: Corresponding US image. . . . .	30
22	3D-printed die casting mold . . . . .	31
23	Air bubbles inside the cured silicone . . . . .	31
24	Final version of mold, used to cast the US-EMG electrode . . . . .	31
25	EMG electrode fixed on US transducer via 3D-printed adapter . . . . .	32
26	Inter electrode distances of the EMG electrode . . . . .	32
27	Schematic of one channel of the developed EMG acquisition device . . . . .	34
28	Final version of the mobile test bench . . . . .	35
29	Schematic of the testbench . . . . .	36
30	Setup for the verification of the mobile test bench . . . . .	36
31	Relation between the average of the measured ADC value and the force, produced by the hung up weight . . . . .	37
32	Setup for the verification of the US-transparent material . . . . .	38
33	Left side: US image of session one, recorded without EMG-adapter. Right side: US image of session two, recorded with the EMG-adapter. The red, dashed lines mark the five depths, used to calculate the histogram curves. . . . .	38
34	Histogram at depth 1 . . . . .	39
35	Histogram at depth 2 . . . . .	39

36	Histogram at depth 3 . . . . .	39
37	Histogram at depth 4 . . . . .	39
38	Histogram at depth 5 . . . . .	39
39	Electrode positioning of the US-transparent EMG-electrode for the biosignal verification . . . . .	40
40	Electrode positioning of the adhesive EMG-electrode for the biosignal verification . . . . .	40
41	Left side: Mean and standard deviation of ten signals per session. Red session: US- transparent EMG electrode, black session: adhesive electrodes. Right side: Hypothesis test. . . . .	41
42	Setup for the Verification of the Developed EMG Acquisition Device. Top right: biowolf-system. Bottom right: Developed EMG Acquisition Device	42
43	Left side: Mean and standard deviation of ten signals per session. Red session: EMG recorded with biowolf, black session: EMG recorded with developed EMG. Right side: Hypothesis test. . . . .	42
44	Force in Nm, measured during MVC on MG . . . . .	43
45	Arrangement of EMG channels during investigation of biceps brachii . . .	44
46	Parallel US and EMG acquisition. At the top: EMG signal of the eight channels. At the bottom, left: US image of biceps brachii during relaxation and right during MVC. . . . .	44
47	Frequency spectrum of the EMG signals, recorded on biceps brachii . . .	45
48	Overview of the 8 HDsEMG signals of biceps brachii during MVC. Blue: HDsEMG signal. Orange: Same signal after Common CoSDonent Analysis.	46
49	Zoomed in HDsEMG signal of all eight channels, recorded on biceps brachii	47
50	Investigation of the behaviour of medial gastrocnemius during a MVC . .	47
51	Parallel US and EMG acquisition. At the top: EMG signal of the eight channels. At the bottom, left: US image of medial gastrocnemius during relaxation and right during MVC. . . . .	48
52	Frequency range of HDsEMG signals, recorded on MG during MVC. Red: Mean frequency. Green: Median frequency. . . . .	49
53	Blue: HDsEMG signal of a MVC, recorded on MG after band pass filtering. Orange: Same signal after a Common CoSDonent Analysis. . . . .	49
54	Zoomed in HDsEMG signal (blue) of channel 1 to 4 during MVC, measured on MG. Green: CCA . . . . .	50
55	Muscle fiber arrangement of biceps brachii (left) and medial gastrocnemius (right) . . . . .	51
56	Green: Normalized torque, measured on TB during MVC. Others: HDsEMG signals standardized to muscle force . . . . .	51

## List of Tables

1	Acoustic impedances of certain materials. Modified from [25] . . . . .	15
2	Different silicone- types, used in this thesis . . . . .	29

3	Older Versions of the mobile test bench . . . . .	34
4	Average ADC value to force relation . . . . .	37